

Joint radar and communications with multicarrier chirp-based waveform

Fredrik Berggren, *Senior Member, IEEE*, and Branislav M. Popović,

We consider a multicarrier chirp-based waveform for joint radar and communication (JRC) systems and derive its time discrete periodic ambiguity function (AF). An advantage of the waveform is that it includes a set of waveform parameters (e.g., chirp rate) which together with the transmit sequence, can be selected to flexibly shape the AF to be thumbtack-like, or to be ridge-like, either along the delay axis or the Doppler axis. These shapes are applicable for different use cases, e.g., target detection or time- and frequency synchronization. The results show that better signal detection performance than OFDM and DFT-s-OFDM can be achieved on channels with large Doppler frequency. Furthermore, it is shown how transmit sequences can be selected in order to achieve 0 dB peak-to-average-power-ratio (PAPR) of the waveform.

Index Terms—Ambiguity function (AF), chirp, joint radar and communication (JRC), peak-to-average-power ratio (PAPR), radar, sequence, synchronization

I. INTRODUCTION

CHIRP waveform with linear frequency modulation (i.e., a linear chirp) appears in various transmission systems and is, e.g., commonly used for radar [1], [2], [3] and ultrasonic positioning [4], as it provides precise ranging and velocity estimation. This stems from its signal properties, which enable efficient pulse-compression together with fulfilling requirements on large time-bandwidth product and low peak-to-average-power ratio (PAPR). A linear chirp has good autocorrelation properties which also makes it suitable as a synchronization signal [5]. Furthermore, multicarrier chirp-based waveforms have been developed for data transmission [6], [7], [8], [9]. Chirp-convolved data transmission (CCDT) is one such a recently proposed multicarrier chirp waveform. This waveform includes parameters (e.g., chirp rate), which when properly selected, exhibit gains over orthogonal frequency division multiplexing (OFDM) and DFT spread OFDM (DFT-s-OFDM) in terms of lower bit- and block error rates on time-frequency selective channels with large Doppler shift [10]. Waveforms which perform well in such scenarios, e.g., for high speed trains, satellites [11] etc., are of interest for 5G systems [12] because communications at velocities up to 350 km/h should be supported, and in some cases even as high as 500 km/h. Thereto, higher frequency bands are introduced in 5G compared to 4G systems [13]. A communication-centric joint radar and communication (JRC) system, leverages on reusing its hardware and waveform, e.g., OFDM, for radar applications [14], [15], [16], [17]. JRC systems using the chirp waveform from [8] have also been suggested [18], [19], [20].

A key tool for waveform synthesis is the ambiguity function (AF), which is a two-dimensional correlation function between a transmitted signal and its received time-delayed and frequency-shifted version. The AF characterizes the output of a matched filter [21] and is a relevant measure for analyzing and synthesizing both synchronization- and radar signals [22], [23]. In this paper, we specifically consider the periodic AF, which mimics the behavior of continuous wave (CW)

radar and pulse radar, cf. [24], [25] and references therein. Periodic multicarrier radar signals, e.g., OFDM radar, could be generated by transmitting multiple OFDM symbols [26] or through an interlaced subcarrier mapping within an OFDM symbol [27]. The periodic AF is particularly convenient to study for waveforms with a cyclic prefix (CP), since the received signal undergoes a cyclic convolution with the channel impulse response. Furthermore, the time discrete AF provides valuable insight into how to design transmit sequences for radar applications [28]. The work in [29], [30], [31] focused on constant amplitude zero autocorrelation (CAZAC) transmit sequences and analyzed the time discrete periodic AF. CAZAC sequences have many desirable properties, e.g., low PAPR due to the constant amplitude (CA) and good time-localization estimation due to zero autocorrelation (ZAC), i.e., they have an ideal autocorrelation function. For example, Zadoff-Chu (ZC) sequences are CAZAC sequences [32] and have been applied as reference signals, synchronization signals and random access preambles in 4G/5G systems, cf. [33], [34]. However, [29], [30], [31] only focused on the transmit sequence and did not assume any waveform, therefore the derived AFs are not directly applicable to multicarrier signals. Herein, we will close this gap and take the waveform into account when determining the AF.

Different shapes of the AF could serve different applications, e.g., a thumbtack-like AF is suitable for estimation of range and velocity for radar, or for determining the timing and the frequency offset for synchronization. With thumbtack-like, we refer to an AF that has a distinct peak at zero time- and frequency offset, while having low sidelobes otherwise. In order to obtain the time- and frequency synchronization with such a shape, the receiver could use a bank of correlators, each corresponding to a certain frequency offset hypothesis, and select the correlator output with largest magnitude [35]. On the other hand, a ridge-like AF allows for detection of the presence of a signal under time delays or Doppler shifts. With ridge-like, we refer to an AF that has a broad peak along either the time- or frequency axis, while having low sidelobes otherwise. It has been shown that OFDM radar can decouple the range and Doppler shift, since it has an AF which is symmetric around

the delay axis and around the frequency axis, respectively [36]. In [37], it was shown that DFT-s-OFDM can produce an AF with lower sidelobes than OFDM. A well-known issue with multicarrier waveforms is the high PAPR which could require substantial power back-off in the transmitter. While this issue has been studied in depth for communications, it is also recognized as important for radar [38], [39]. DFT-s-OFDM is a low-PAPR waveform which is supported in 4G/5G, cf. [33]. It has also been suggested for radar [27], [37] and due to the DFT-precoder, the PAPR is several dB smaller than for OFDM.

In this paper, a multicarrier chirp-based waveform, CCDT, is considered for radar and synchronization applications. It has been reported to outperform OFDM and DFT-s-OFDM for data transmission and would thus be a candidate waveform for JRC. Importantly, it has been shown that the waveforms in [8], [10] can be represented as DFT-s-OFDM with a unitary frequency domain chirp filter. This is a big advantage since DFT-s-OFDM is already implemented in the 4G/5G terminals, and introducing CCDT could be simple and not require significant complexity increase. Furthermore, CCDT is more flexible than OFDM and DFT-s-OFDM since, as will be shown herein, with a judicious choice of the transmit sequence and parameters (e.g., the chirp rate), the AF could be shaped to be either thumbtack-like or ridge-like.

Designing radar signals such that the AF is shaped to the environment and to a certain desired form over a given range-Doppler region, is a well-known problem, cf. [40], [41] and references therein. Flexible AF shaping is also useful for synchronization purposes, e.g., in the initial synchronization between a terminal and the base station, the AF could be ridge-like, first in the Doppler domain, to allow the terminal to perform time-domain synchronization acquisition, and then in the delay domain, to allow the terminal to perform frequency-domain synchronization acquisition. Once the synchronization acquisition is achieved the AF of the transmitted signal could be switched to thumbtack-like, to enhance time- and frequency synchronization tracking in the terminal. It should be noted that current systems, e.g., 3GPP LTE and NR, do not exhibit such flexibility.

The contributions of the paper are summarized as follows.

- *Ambiguity function:* We derive the AF on closed-form for an arbitrary transmit sequence and show how it is shaped by the chirp rate and the transmit sequence. It is shown that the AF becomes the convolution in the time domain between the AF of the basis functions of the multicarrier chirp-based waveform and the AF of the transmit sequence. Moreover, we derive the AF under arbitrary sampling rate and non-integer frequency offsets.
- *Transmit sequence:* We then derive the AF assuming specific transmit sequences, i.e., a ZC sequence, DFT sequence or m-sequence. It is shown that these can shape the AF to be either thumbtack-like or ridge-like.
- *Comparison to OFDM and DFT-s-OFDM:* We derive the AFs for OFDM and DFT-s-OFDM and compare to that of CCDT. The results show that CCDT has better detection performance on channels with large Doppler frequency. Moreover, we show that a thumbtack-like

shape is achieved from random modulation symbols. This is typically the case for JRC, where random but known data symbols constitute the transmit sequence.

- *Low PAPR:* We show that ZC and DFT transmit sequences result in a signal with 0 dB PAPR.

The rest of the paper is organized as follows. In Section II, the AF of CCDT and its properties are derived. Comparison to OFDM and DFT-s-OFDM is contained in Section III. The PAPR properties are presented in Section IV. Numerical evaluation of synchronization and detection performance is contained in Section V, the paper is concluded in Section VI and the mathematical proofs are contained in Appendix A-F.

II. SIGNAL PROPERTIES

A. Chirp-Convolved Data Transmission

Consider the CCDT waveform for $0 \leq t < T$ defined by

$$s(t) = \sum_{m=0}^{N-1} x[m]g\left(t - \frac{mT}{N}\right) \quad (1)$$

where $x[m]$, $m = 0, 1, \dots, N-1$, is taken from a set of (real- or complex valued) modulation symbols. These symbols either correspond to random data or a pre-determined transmit sequence. The pulse shape (or basis function) $g(t)$ is periodic such that the time discrete representation of (1) for $t = nT/N$, for a symbol with samples $n = 0, 1, \dots, N-1$ is defined by [10]

$$s[n] = \sum_{m=0}^{N-1} x[m]g[n-m] \quad (2)$$

$$g[k] = \frac{1}{\sqrt{N}} e^{-j\frac{2\pi}{N}(\alpha k^2 + \beta k + \gamma)} \quad (3)$$

$$\gcd(2\alpha, N) = 1 \quad (4)$$

$$\alpha N + \beta \in \mathbb{Z} \quad (5)$$

where α, β and γ are real-valued, \mathbb{Z} is the set of integers, and $\gcd(A, B)$ is the greatest common divisor of the integers A and B . We refer to α as the chirp rate. A CP of length N_{CP} can be inserted by defining (2) for $n = -N_{CP}, -N_{CP} + 1, \dots, -1$. The set of basis functions $g[n-m]$ are generated from cyclic time-shifts of (3). It has been shown that the conditions (4) and (5) imply that (3) is a CAZAC sequence, i.e., the basis functions are orthogonal. It has also been shown that the CCDT waveform can be represented as DFT-s-OFDM with an additional chirp filter prior to the Inverse DFT (IDFT) [10]. Therefore, we will also make use of the alternative representation of (2)-(5) given by:

$$s[n] = \frac{1}{\sqrt{N}} \sum_{m=0}^{N-1} G[m]X[m]e^{j\frac{2\pi}{N}mn} \quad (6)$$

$$G[m] = \sum_{k=0}^{N-1} g[k]e^{-j\frac{2\pi}{N}km} \quad (7)$$

$$X[m] = \frac{1}{\sqrt{N}} \sum_{k=0}^{N-1} x[k]e^{-j\frac{2\pi}{N}km} \quad (8)$$

It can be shown that the DFT of a CAZAC sequence is a CAZAC sequence [30]. Thus $G[m]$ has CA and the filter reduces to N phase shifts. Due to $G[m]$ in (6), modulation

symbols become multiplexed in both the time- and frequency domain, thus offering diversity gains in time-frequency selective channels. This is in contrast to OFDM where modulation symbols are frequency multiplexed, and to DFT-s-OFDM, where modulation symbols are time-multiplexed.

B. Time Discrete Periodic Ambiguity Function

We consider the sampled low-pass equivalent signal for this analysis. For a time discrete signal $s[n]$, the periodic AF is defined as [30]

$$\chi(\Delta, \tau) \stackrel{\text{def}}{=} \frac{1}{N} \sum_{n=0}^{N-1} s[n] s^*[n + \tau \pmod{N}] e^{j \frac{2\pi}{N} \Delta n} \quad (9)$$

for a frequency offset $\Delta \in \mathbb{Z}$ and time-delay $\tau \in \mathbb{Z}$, where $(\cdot)^*$ denotes complex-conjugate and $(\text{mod } N)$ is the modulo- N operator. It is straightforward to verify that (9) has a period of N , i.e., $\chi(\Delta, \tau) = \chi(\Delta + N, \tau) = \chi(\Delta, \tau + N) = \chi(\Delta + N, \tau + N)$. The AF (9) could be computed efficiently by the Inverse DFT (IDFT) for each τ of the product sequence $s[n] s^*[n + \tau \pmod{N}]$. In Sec. II-G, the case with non-integer frequency offsets Δ is discussed. We obtain the following main result.

Property 1. The ambiguity function is:

$$\chi(\Delta, \tau) = C \sum_{m=0}^{N-1} x \left[m - \tau + \frac{r_0 N - \Delta}{2\alpha} \pmod{N} \right] x^*[m] \times e^{j \frac{2\pi}{N} \Delta m} \quad (10)$$

$$C = \sqrt{N} g^*[\tau] g[\tau + \Delta/2\alpha] g[-r_0 N/2\alpha] \times e^{j \frac{2\pi}{N} \tau} e^{j \pi \frac{r_0 \Delta}{\alpha}} \quad (11)$$

$$r_0 = \frac{2\alpha k_0 + \Delta + 2\alpha\tau}{N} \quad (12)$$

$$2\alpha k_0 \equiv -\Delta - 2\alpha\tau \pmod{N} \quad (13)$$

$$k_0 \in \{0, 1, \dots, N-1\} \quad (14)$$

Hence, except for the complex-valued scaling constant C , the AF of $s[n]$ simply reduces to the periodic AF of $x[m]$ at a delay $\epsilon = -\tau + (r_0 N - \Delta)/2\alpha$, which is a function of both τ and Δ . Moreover, the magnitude of (10) is independent of β and γ , while the chirp rate α determines the delay. Thus, the AF can be shaped by the transmit sequence $x[m]$ and the parameter α . In the following, we will only consider the modulus AF, since the phase of C is typically not detected in the receiver. The zero Doppler cut AF is obtained by setting $\Delta = 0$ in (10) and observing that $r_0 = 0$ is a solution to (57). Hence, the modulus AF can be simplified as

$$|\chi(\Delta = 0, \tau)| = \left| \sum_{m=0}^{N-1} x[m] x^*[m + \tau \pmod{N}] \right| \quad (15)$$

which is the periodic autocorrelation function of the transmit sequence $x[m]$. Notably, it is not dependent of α and is thus only shaped by the transmit sequence.

The location and magnitude of sidelobes will depend on the transmit sequence. However, a general property is that, for any $x[m]$ with CA, the AF is zero in certain locations of the $\Delta - \tau$ plane. Define the Kronecker delta function as $\delta[k] = 1$ for $k = 0$ and $\delta[k] = 0$ for $k \neq 0$, then the following property holds.

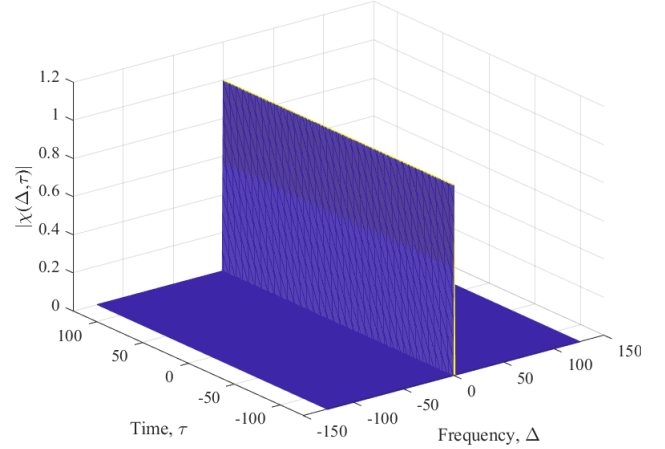


Fig. 1. Modulus AF using a DFT sequence of length $N = 127$.

Property 2. If $|x[m]| = 1$ and $\Delta + 2\alpha\tau \equiv 0 \pmod{N}$, then $|\chi(\Delta, \tau)| = \delta[\Delta]$.

A CAZAC sequence $x[m]$ fulfills the following CA and ZAC conditions:

$$|x[m]| = 1 \quad (16)$$

$$\frac{1}{N} \sum_{m=0}^{N-1} x[m] x^*[m + \tau \pmod{N}] = \delta[\tau] \quad (17)$$

It follows from Property 1 with $\Delta = 0$ and (15) that, if $x[m]$ has an ideal autocorrelation function, i.e., fulfills the ZAC property (17), also $s[n]$ will be a ZAC sequence. However, even if $x[m]$ has CA, it does not generally guarantee that $s[n]$ has CA. Albeit, for some sequences $x[m]$ it is fulfilled, which we discuss in Sec. V. A general property for CCDT using CAZAC sequences is given by the following.

Property 3. If $x[m]$ is a CAZAC sequence, then $\sum_{\tau=0}^{N-1} |\chi(\Delta, \tau)|^2 = 1$.

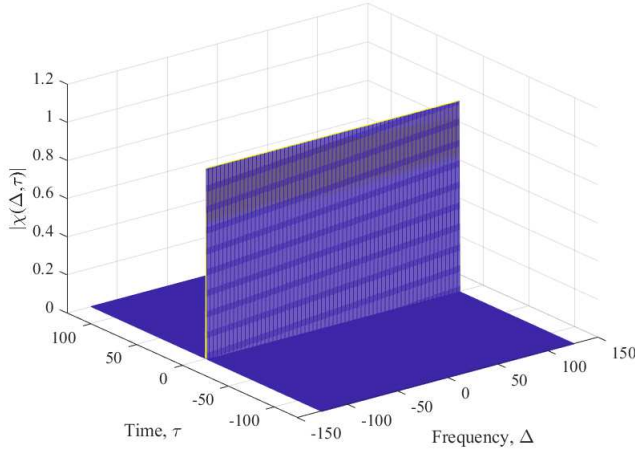
This property can be used to determine a bound on the sidelobes of the AF. For example, if there exists a τ_0 for which $|\chi(\Delta, \tau_0)| = 1$, then $|\chi(\Delta, \tau_1)| = 0$ for any $\tau_1 \neq \tau_0$.

C. Ridge-like Ambiguity Function

A ridge-like AF makes it possible to detect the presence of a signal by a matched filter under any time delay or frequency shift. According to Property 4, a ridge-like AF is generated from a DFT sequence, which is illustrated in Fig. 1. The ridge is along the τ -axis, i.e., τ and Δ are decoupled.

Property 4. If $x_k[m] = e^{j \frac{2\pi}{N} km}$ for $k = 0, 1, \dots, N-1$, then $|\chi(\Delta, \tau)| = \delta[\Delta]$.

In this case, the ridge lies along the time axis and thus the detection of the presence of a signal with any time delay could be performed by a matched filter, which will produce the maximum value for any time delay. This type of AF could also be applicable for estimating the frequency offset, e.g., by fixing a time delay and performing matched filtering with one filter for each frequency offset hypothesis. Thereby, the frequency

Fig. 2. Modulus AF using a ZC sequence of length $N = 127$.

offset is determined from the hypothesis that produces the largest matched filter output.

A benefit of the CCDT is the ability to select α . As shown by Property 5, the AF can be shaped such that the ridge is rotated 90 degrees in the $\Delta - \tau$ plane by using a ZC sequence with root index $u = 2\alpha$, which is illustrated in Fig. 2.

Property 5. If $x_u[m] = e^{j\frac{\pi}{N}um(m+1)}$, where N is odd and $u = 2\alpha$, then $|\chi(\Delta, \tau)| = \delta[\tau]$

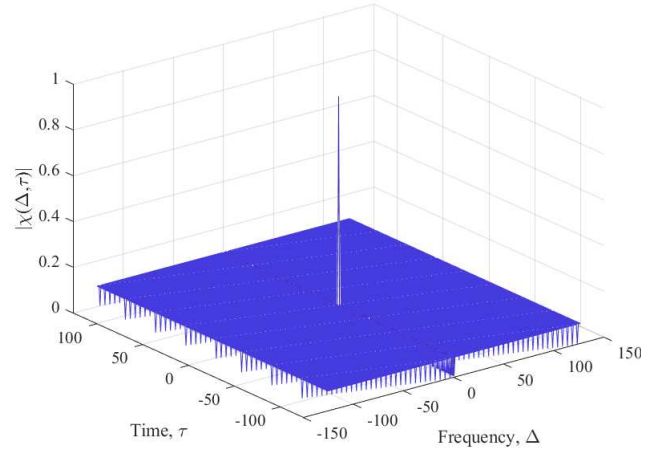
In this case, the ridge lies along the frequency axis and thus the detection of the presence of a signal with any Doppler shift could be performed by a matched filter, which will produce the maximum value for any Doppler shift. A similar property can be found when N is even and $x_u[m] = e^{j\frac{\pi}{N}um^2}$, which is omitted here for brevity. Since a ZC sequence is a CAZAC sequence, Property 5 could alternatively be proven using Property 3 and noting that when $u = 2\alpha$ and $\tau = 0$, (60) holds for all Δ , i.e., $|\chi(\Delta, \tau = 0)| = 1$, and thus $|\chi(\Delta, \tau \neq 0)| = 0$.

D. Thumbtack-like Ambiguity Function

A thumbtack-like AF is characterized by having a small value of $|\chi(\Delta, \tau)|$ for $\Delta \neq 0$ and $\tau \neq 0$. This allows unambiguous time- and frequency synchronization for communications or range and velocity estimation for radar. An interesting case is where a maximum length sequence, aka. m-sequence, is used. The m-sequence is defined for $N = 2^p - 1$ for a positive integer p , $x[m] \in \{-1, 1\}$ and its periodic autocorrelation function is

$$\rho(\tau) = \frac{1}{N} \sum_{m=0}^{N-1} x[m]x[m + \tau \pmod{N}] = \begin{cases} 1, & \tau = 0 \\ -\frac{1}{N}, & \tau \neq 0. \end{cases} \quad (18)$$

The modulus AF is given by Property 6, which is illustrated in Fig. 3.

Fig. 3. Modulus AF where an m-sequence of length $N = 127$ is used, and $\alpha = 2$ and $\beta = 1$.

Property 6. If $x[m]$ is an m-sequence, then

$$|\chi(\Delta, \tau)| = \begin{cases} 1, & \Delta = 0, \tau = 0 \\ \frac{1}{N}, & \Delta = 0, \tau \neq 0 \\ 0, & \Delta + 2\alpha\tau \equiv 0 \pmod{N} \\ \sqrt{(N+1)}/N, & \text{otherwise.} \end{cases} \quad (19)$$

E. Ambiguity function with random data

For JRC systems, $x[m]$ may consist of random, but known, modulation symbols, e.g., used for transmitting data. It is therefore important that the expected AF has good properties. Analysis of the statistical properties of the AF has similarly been performed for noise radar systems, where the transmitted signal is obtained from a stochastic process [42]. Suppose $x[m] = e^{-j2\pi\phi'_m}$ and ϕ'_m is chosen independently and randomly from a uniform distribution $\phi'_m \in [0, 1)$. Let $\epsilon = -\tau + (r_0N - \Delta)/2\alpha \neq 0$, then it follows that for $\Delta \neq 0$ and $\tau \neq 0$, $x[m]x^*[m + \epsilon \pmod{N}] = e^{j2\pi(\phi'_{m+\epsilon \pmod{N}} - \phi'_m)}$ and $\phi_m = \phi'_{m+\epsilon \pmod{N}} - \phi'_m$ becomes a random variable. The probability density function of the difference between two uniform random variables can be determined as

$$f_{\phi_m}(x) = \begin{cases} x + 1, & -1 < x \leq 0 \\ 1 - x, & 0 < x < 1. \end{cases} \quad (20)$$

Utilizing $\int x e^{ax} dx = (ax - 1)a^{-2}e^{ax}$, we can obtain the expectation value, $\mathbb{E}[\cdot]$, of (10) as

$$\begin{aligned} |\mathbb{E}[\chi(\Delta \neq 0, \tau \neq 0)]| &= \frac{1}{N} \left| \sum_{m=0}^{N-1} \mathbb{E}[e^{j2\pi\phi_m}] e^{j\frac{2\pi}{N}\Delta m} \right| \\ &= \frac{1}{N} \left| \sum_{m=0}^{N-1} \left(\int_{-1}^1 f_{\phi_m}(\phi) e^{j2\pi\phi} d\phi \right) \right. \\ &\quad \left. \times e^{j\frac{2\pi}{N}\Delta m} \right| \\ &= 0. \end{aligned} \quad (21)$$

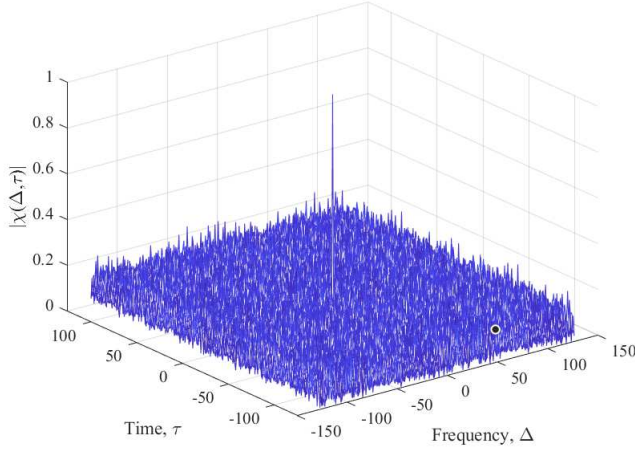


Fig. 4. Example of a realization of the modulus AF where $N = 127$ random unitary modulation symbols are used and $\alpha = 2$ and $\beta = 1$.

Thus the expectation value of the modulus AF exhibits a thumbtack-like shape and good detection performance in average sense is expected. Fig. 4 shows one realization of the modulus AF where the modulation symbols are randomly generated on the unit circle. Moreover, if the modulation symbols are chosen independently and randomly from an M -PSK constellation, $\phi'_m = e^{j\frac{2\pi}{M}p}$ with $\Pr[p = p'] = 1/M$ and $p = 0, 1, \dots, M-1$, then ϕ_m will correspond to the angle of one of the constellation points with uniform probability. Therefore, the expectation value of the AF will be thumbtack-like since, by using (55)

$$\begin{aligned} |\mathbb{E}[\chi(\Delta \neq 0, \tau \neq 0)]| &= \frac{1}{N} \left| \sum_{m=0}^{N-1} \mathbb{E}[e^{j2\pi\phi_m}] e^{j\frac{2\pi}{N}\Delta m} \right| \\ &= \frac{1}{N} \left| \sum_{m=0}^{N-1} \left(\sum_{p=0}^{M-1} \frac{1}{M} e^{j\frac{2\pi}{M}p} \right) e^{j\frac{2\pi}{N}\Delta m} \right| \\ &= 0. \end{aligned} \quad (22)$$

Thus CCDT would be suitable for JRC, where the $x[m]$ represents modulation symbols, which are known but not pre-determined.

F. Ambiguity Function With Upsampling

The AF for an upsampled signal can be obtained from (6) by replacing N with Q ($Q > N$) in the exponential function. As shown in Appendix C, when $Q/N \in \mathbb{Z}$, the AF becomes

$$\begin{aligned} \chi(\Delta, \tau) &= \frac{N}{Q} \sum_{v=0}^{N-1} \sum_{w=0}^{N-1} \chi_g(\Delta, v) \chi_x(\Delta, w) \\ &\quad \times \frac{\sin\left(\pi\left(v+w-\frac{N}{Q}\tau\right)\right)}{\sin\left(\frac{\pi\left(v+w-\frac{N}{Q}\tau\right)}{N}\right)} e^{\frac{\pi(N-1)\left(v+w-\frac{N}{Q}\tau\right)}{N}} \end{aligned} \quad (23)$$

where $\chi_g(\Delta, \tau)$ and $\chi_x(\Delta, \tau)$ are the AFs of the sequences $g[k]$ and $x[m]$, respectively. Fig. 5 shows the modulus AF with $Q = 10N$, using an m-sequence for $x[m]$. This should

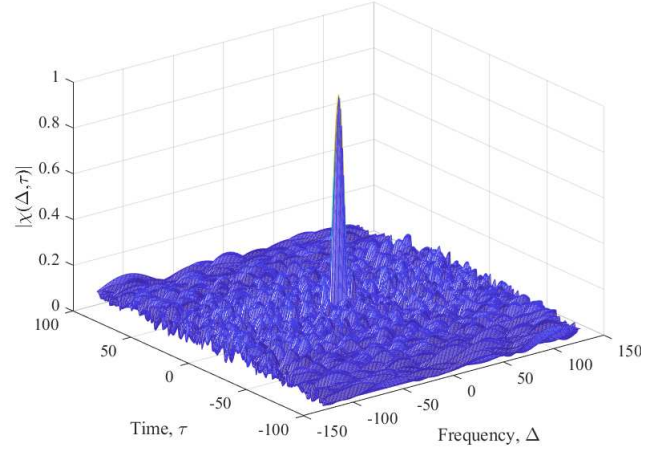


Fig. 5. Modulus AF with $Q/N = 10$ times upsampling, where an m-sequence of length $N = 127$ is used, and $\alpha = 2$ and $\beta = 1$.

be compared to Fig. 3 (i.e., where $Q = N$) and it can be seen that the thumbtack-like characteristics are maintained with upsampling. An interesting case of (23) is when $Q = N$, which gives an alternative expression for the AF with no upsampling. From Appendix C, we obtain

$$\chi(\Delta, \tau) = N \sum_{v=0}^{N-1} \chi_g(\Delta, v) \chi_x(\Delta, \tau - v). \quad (24)$$

In other words, the convolution over the delays of the AFs $\chi_g(\Delta, \tau)$ and $\chi_x(\Delta, \tau)$ gives the AF for $s[n]$. The AF of (10) could equivalently be obtained by inserting $\chi_g(\Delta, \tau)$ and $\chi_x(\Delta, \tau)$ in (24), which is shown in Appendix D.

G. Ambiguity Function With Non-integer Frequency Offset

The AF with upsampling and non-integer frequency offset are given by (64) and (65) in Appendix C. Further simplification can be done for the case without upsampling by using this identity for an arbitrary p

$$\sum_{n=0}^{N-1} e^{j\frac{2\pi}{N}np} = \frac{\sin(\pi p)}{\sin\left(\frac{\pi p}{N}\right)} e^{j\frac{\pi(N-1)p}{N}} \quad (25)$$

in (54) with $p = \Delta - 2\alpha(m-k) + 2\alpha\tau$. Then the AF becomes as follows.

$$\begin{aligned} \chi(\Delta, \tau) &= \sum_{m=0}^{N-1} \sum_{k=0}^{N-1} x[k] x^*[m] e^{-j\frac{2\pi}{N}(\alpha(k^2-m^2)+\beta(m-k)+2\alpha\tau m)} \\ &\quad \times C_0 \frac{\sin\left(\pi\left(\Delta - 2\alpha(m-k) + 2\alpha\tau\right)\right)}{\sin\left(\frac{\pi\left(\Delta - 2\alpha(m-k) + 2\alpha\tau\right)}{N}\right)} \\ &\quad \times e^{j\frac{\pi(N-1)\left(\Delta - 2\alpha(m-k) + 2\alpha\tau\right)}{N}} \end{aligned} \quad (26)$$

Fig. 6 shows the modulus AF (26) when Δ is assumed in steps of 0.1, and similarly to Fig. 3, the thumbtack-like shape is maintained.

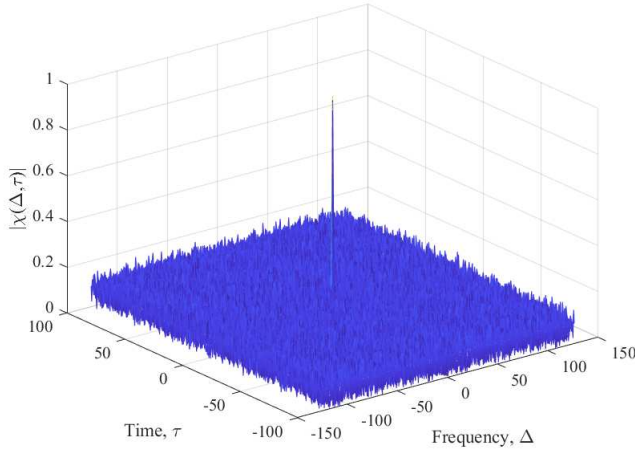


Fig. 6. Modulus AF for non-integer frequency offset where binary modulation symbols from an m-sequence of length $N = 127$, and $\alpha = 2$ and $\beta = 1$.

III. COMPARISON WITH OFDM AND DFT-s-OFDM

As mentioned in Sec. II.A, CCDT is utilizing features of both OFDM (i.e., transmitting a modulation symbol over the whole OFDM symbol) and DFT-s-OFDM (i.e., transmitting a modulation symbol over the whole bandwidth). Therefore, we will compare the AF of CCDT with those of OFDM and DFT-s-OFDM. Such expressions appear not to be available in the literature, and for completeness we will derive the AFs with different transmit sequences.

A. OFDM

The OFDM signal is defined by

$$s[n] = \frac{1}{\sqrt{N}} \sum_{k=0}^{N-1} x[k] e^{j \frac{2\pi}{N} kn} \quad (27)$$

which when inserted in (9) yields

$$\begin{aligned} |\chi(\Delta, \tau)| &= \frac{1}{N^2} \left| \sum_{m=0}^{N-1} \sum_{k=0}^{N-1} x[m] x^*[k] e^{-j \frac{2\pi}{N} \tau k} \right. \\ &\quad \left. \times \sum_{n=0}^{N-1} e^{j \frac{2\pi}{N} n(m-k+\Delta)} \right| \\ &= \frac{1}{N} \left| \sum_{m=0}^{N-1} x[m - \Delta \pmod{N}] x^*[m] e^{-j \frac{2\pi}{N} \tau m} \right| \end{aligned} \quad (28)$$

since the inner sum is equal to $N\delta[m-k+\Delta \pmod{N}]$ due to (55). There are several differences between (10) and (28), i.e., it is the periodic AF of $x[m]$ but with Δ and τ interchanged compared to (10). The zero delay cut AF follows directly from (28) as

$$|\chi(\Delta, \tau = 0)| = \frac{1}{N} \left| \sum_{m=0}^{N-1} x[m - \Delta \pmod{N}] x^*[m] \right| \quad (29)$$

and is thus the periodic autocorrelation function of $x[m]$. The zero Doppler cut AF is an impulse as shown by the following. *Property 7.* When $|x[m]| = 1$, then $|\chi(\Delta = 0, \tau)| = \delta[\tau]$.

The property implies that an OFDM signal with constant modulus modulation symbols has ideal periodic autocorrelation, which was also shown in [43].

A ridge-like shape could be achieved from a DFT sequence according to the following property. It should be noted that this ridge is the same as for CCDT with ZC sequence (i.e., Property 5 and Fig. 2).

Property 8. If $x_k[m] = e^{j \frac{2\pi}{N} km}$, for $k = 0, 1, \dots, N-1$, then $|\chi(\Delta, \tau)| = \delta[\tau]$.

In contrast to CCDT, a ZC sequence does not produce an AF with a ridge with decoupled τ and Δ parameters, which is shown by the following property.

Property 9. If $x_u[m] = e^{j \frac{2\pi}{N} um(m+1)}$, N is odd and $u = 1, \dots, N-1$, then $|\chi(\Delta, \tau)| = \delta[u\Delta + \tau \pmod{N}]$.

Notably, a ZC sequence was used for the primary synchronization signal (PSS) in 3GPP LTE. However, it was replaced by an m-sequence in 3GPP NR, much due to the undesirable sidelobes and the coupling of τ and Δ in the AF.

B. DFT-s-OFDM

The signal is defined by inserting a DFT-precoder prior to the OFDM modulator such that

$$\begin{aligned} s[n] &= \frac{1}{\sqrt{N}} \sum_{k=0}^{N-1} \frac{1}{\sqrt{N}} \sum_{l=0}^{N-1} x[l] e^{-j \frac{2\pi kl}{N}} e^{j \frac{2\pi kn}{N}} \\ &= x[n] \end{aligned} \quad (30)$$

which when inserted in (9) yields

$$|\chi(\Delta, \tau)| = \frac{1}{N} \left| \sum_{m=0}^{N-1} x[m - \tau \pmod{N}] x^*[m] e^{j \frac{2\pi}{N} \Delta m} \right|. \quad (31)$$

The similarity with (10) is that (31) is also the periodic ambiguity autocorrelation function of $x[m]$, but at a delay, τ , which is independent of Δ . The zero Doppler cut AF follows directly from (31) as

$$|\chi(\Delta = 0, \tau)| = \frac{1}{N} \left| \sum_{m=0}^{N-1} x[m - \tau \pmod{N}] x^*[m] \right| \quad (32)$$

and is thus the periodic autocorrelation function of $x[m]$. The zero delay cut AF is an impulse as shown by the following property.

Property 10. When $|x[m]| = 1$, then $|\chi(\Delta, \tau = 0)| = \delta[\Delta]$

This is the corresponding property of Property 7 for OFDM but with Δ replacing τ . Moreover, a ridge-like AF can be produced, similarly as for CCDT with a DFT sequence (i.e., Property 4 and Fig. 1).

Property 11. If $x_k[m] = e^{j \frac{2\pi}{N} km}$, for $k = 0, 1, \dots, N-1$, then $|\chi(\Delta, \tau)| = \delta[\Delta]$.

As given by Property 9 for OFDM, a ZC sequence does not produce an AF with a ridge with decoupled τ and Δ parameters. This is also the case for DFT-s-OFDM, which is shown by the following property.

Property 12. If $x_u[m] = e^{j \frac{2\pi}{N} um(m+1)}$, N is odd and $u = 1, \dots, N-1$, then $|\chi(\Delta, \tau)| = \delta[\Delta - \tau u \pmod{N}]$.

C. Comparison with CCDT

Both Property 7 and Property 10 are different from CCDT, where Property 2 is determining the locations of zeros in the $\Delta - \tau$ plane. The AF of OFDM can be obtained from that of DFT-s-OFDM by exchanging τ with Δ and ridge-like shapes are possible from DFT sequences, but not ZC sequences. Furthermore, by using (28) or (31), it will be possible to use the same steps as for (20)-(22) and show that when random unitary modulation symbols are used, the expected AF is thumbtack-like. Hence, the whole family of CCDT, OFDM and DFT-s-OFDM waveforms may be suited for JRC systems.

IV. PEAK-TO-AVERAGE-POWER-RATIO

A low PAPR allows less power back-off in the transmitter and thus has benefits for coverage of the transmitted signal. If $|x[m]| = 1$, it can be shown using (2) that $\frac{1}{N} \sum_{n=0}^{N-1} |s[n]|^2 = 1$. Thus, the PAPR is defined as:

$$\text{PAPR} = 10 \log_{10} \left(\max_{0 \leq n \leq N-1} |s[n]|^2 \right)$$

A CA sequence has by definition 0 dB PAPR, but that does not generally guarantee that $s[n]$ has 0 dB PAPR. However, the following properties for ZC and DFT sequences show that it is the case for CCDT.

Property 13. If $x_u[m] = e^{j \frac{\pi}{N} u m(m+1)}$, where N is odd prime and $\text{gcd}(u, N) = 1$,

$$\text{PAPR} = \begin{cases} 10 \log_{10} N, & u = 2\alpha \\ 0, & u \neq 2\alpha. \end{cases}$$

From (78), it follows that when $u = 2\alpha$ there exists an $n = n_0$ fulfilling $\alpha + 2\alpha n_0 + \beta \equiv 0 \pmod{N}$ and the signal becomes

$$s[n] = \begin{cases} \sqrt{N} e^{-j \frac{2\pi}{N} (\alpha n_0^2 + \beta n_0 + \gamma)}, & n = n_0 \\ 0, & n \neq n_0. \end{cases} \quad (33)$$

Thus, the PAPR of $10 \log_{10} N$ for $u = 2\alpha$ is a consequence of that the signal contains all energy in one sample, n_0 . For any DFT sequence, $\text{PAPR} = 0$ dB, as shown by the following property.

Property 14. If $x_k[m] = e^{j \frac{2\pi}{N} k m}$, for $k = 0, 1, \dots, N-1$, $\text{PAPR} = 0$ dB.

In practice, the PAPR is measured on the time continuous signal. We model this by upsampling $s[n]$, which implies that the PAPR will become larger than 0 dB. Fig. 7 shows the complementary cumulative distribution function (CCDF) of PAPR with $Q = 4N$, using a ZC sequence of length $N = 127$ with different root indices u . With the exception of the PAPR of $10 \log_{10} N$ for CCDT with $u = 2\alpha$, the PAPRs are comparable. It should be noted that since the DFT of a cyclically-shifted ZC sequence produces the output sequence which is a complex-conjugated and permuted version of the DFT input sequence [44]. Thus the PAPR curve for DFT-s-OFDM is the same as for OFDM.

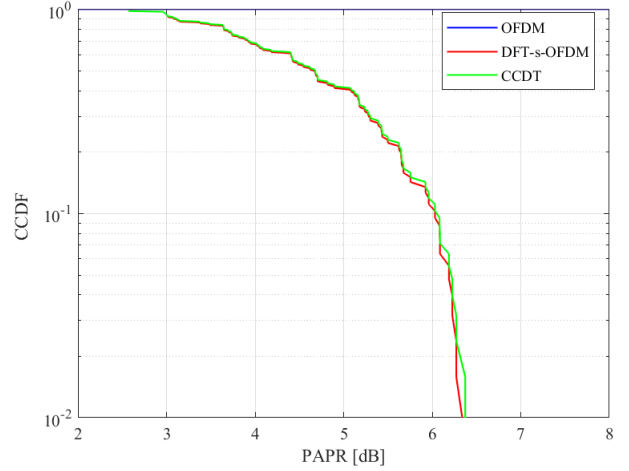


Fig. 7. Complementary CDF of the PAPR where a ZC sequence of length $N = 127$ is used, for OFDM, DFT-s-OFDM and CCDT with $\alpha = 2$ and $\beta = 1$.

TABLE I
LIST OF EVALUATION PARAMETERS AND MODELS.

Parameter	Value
Subcarrier spacing	$f_{\text{SCS}} = 15$ kHz
Carrier frequency	$f_c = 6$ GHz
Modulation sequence	m-sequence, $N = 127$
Channel model	Vehicular A; 0 – 500 km/h Clarke's model, $P = 5$ paths

V. DETECTION PERFORMANCE

A. Synchronization

Let us assume a time discrete channel model with the assumptions in Table I as

$$h[n] = \sum_{l=0}^{L-1} \sqrt{\mathcal{P}_l} \tilde{h}_l[n] \delta[n - \tau_l] \quad (34)$$

where the relative channel tap powers \mathcal{P}_l and sample delays τ_l are obtained from a Vehicular A channel according to Table II, assuming the sampling frequency $f_s = N f_{\text{SCS}}$. We are considering a time-variant channel using Clarke's two-dimensional isotropic scattering Rayleigh fading model [45]

$$\tilde{h}_l[n] = \frac{1}{\sqrt{P}} \sum_{p=1}^P e^{j(2\pi f_D n \cos \theta_p + \phi_p)} \quad (35)$$

where P is the number of propagation paths per channel tap, $f_D = \frac{v}{c} f_c$ is the maximum Doppler frequency, v is the velocity, c is the speed of light, f_c the carrier frequency and θ_p and ϕ_p are the angle of arrival and initial phase of the p th propagation

TABLE II
POWER DELAY PROFILE OF THE TIME DISCRETE VEHICULAR A CHANNEL ASSUMING $f_s = N f_{\text{SCS}}$ WITH $N = 127$ AND $f_{\text{SCS}} = 15$ KHZ.

τ_l	0	1	2	3	5
\mathcal{P}_l	0.4850	0.4463	0.0485	0.0153	0.0049

path, respectively. Both θ_p and ϕ_p are uniformly distributed over $[-\pi, \pi)$ for all p and they are mutually independent. For $f_D \neq 0$, the channel (35) varies over a symbol and the subcarriers are no longer orthogonal in the receiver and inter-carrier interference (ICI) occurs.

A CP of length $N_{CP} \geq L$ is attached to $s[n]$ and the received signal $r[n]$, is obtained from convolution with $h[n]$, and adding additive white Gaussian noise (AWGN), $w[n]$. After removing the CP, the signal can be expressed as follows.

$$r[n] = \sum_{l=0}^{L-1} \sqrt{\mathcal{P}_l} \tilde{h}_l[n] s[n - \tau_l \pmod{N}] + w[n] \quad (36)$$

The periodic correlation is then performed at the sample rate $f_s = N f_{SCS}$ as follows to determine the timing sample τ^* .

$$\rho(\tau) = \left| \frac{1}{N} \sum_{n=0}^{N-1} r[n] s^*[n - \tau \pmod{N}] \right| \quad (37)$$

$$\tau^* = \arg \max_{\tau \in \{0, 1, \dots, N-1\}} \rho(\tau) \quad (38)$$

By defining the set of time delay samples of the channel $\mathcal{T} = \{\tau_0, \tau_1, \dots, \tau_{L-1}\}$, the probability of misdetection, P_{md} , is defined by the events of not detecting the received signal on any of the delays in \mathcal{T} .

$$P_{md} = \Pr[\tau^* \notin \mathcal{T}] \quad (39)$$

Determining (39) on closed-form appears to be a formidable task and we resort to Monte Carlo simulations for its evaluation, for velocities in the range 0 – 500 km/h. At $f_c = 6$ GHz, a velocity of 500 km/h corresponds to a Doppler frequency $f_D = 2.78$ kHz or, equivalently, $f_D = 0.185 f_{SCS}$. The effect of the Doppler would be the same if f_{SCS} scales with f_c , e.g., using $f_{SCS} = 60$ kHz at $f_c = 24$ GHz. We assume an m-sequence of length $N = 127$, which is also used as primary synchronization signal sequence in 3GPP NR [33]. Fig. 8 shows that CCDT performs slightly better than OFDM and DFT-s-OFDM as the velocity increases. This is corroborated by a slightly less standard deviation of τ^* as shown in Fig. 9. The mean of τ^* approached 0.5 for all schemes, which is expected since according to Table II, the power \mathcal{P}_l for the taps $\tau_l = 0$ and $\tau_l = 1$ are similar.

Synchronization signals may need to be detected under large frequency offsets. For example, during initial cell acquisition, prior to when the mobile device has established frequency synchronization with the base station, an oscillator inaccuracy in the order of 10 ppm is typically assumed [11]. We introduce a frequency offset of f_o Hz between the transmitter and receiver as

$$r[n] = \sum_{l=0}^{L-1} \sqrt{\mathcal{P}_l} \tilde{h}_l[n] e^{j \frac{2\pi}{N} \frac{f_o}{f_{SCS}} n} s[n - \tau_l \pmod{N}] + w[n] \quad (40)$$

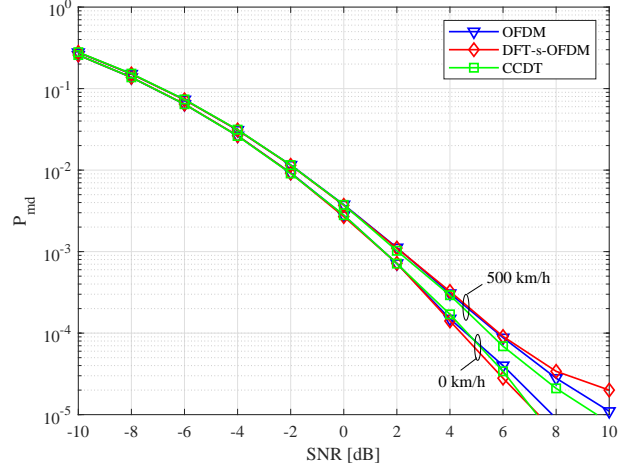


Fig. 8. Probability of misdetection using an m-sequence of length $N = 127$ for different velocities on a Vehicular A channel, for subcarrier spacing $f_{SCS} = 15$ kHz, carrier frequency $f_c = 6$ GHz, for the waveforms OFDM, DFT-s-OFDM and CCDT with $\alpha = -2$ and $\beta = -2$.

TABLE III
REQUIRED SNR [dB] FOR $P_{md} = 10^{-4}$, FOR DIFFERENT NUMBER OF FREQUENCY HYPOTHESES.

Velocity	100 km/h			350 km/h		
	\mathcal{D}_3	\mathcal{D}_5	\mathcal{D}_7	\mathcal{D}_3	\mathcal{D}_5	\mathcal{D}_7
OFDM	6.20	5.95	5.95	6.00	5.40	5.30
DFT-s-OFDM	6.20	5.85	5.80	6.00	5.35	5.20
CCDT	6.20	5.85	5.85	5.70	5.25	5.05

and a bank of correlators, each corresponding to a frequency offset hypothesis Δ_f , is used for signal detection.

$$\rho(\tau_f, \Delta_f) = \left| \frac{1}{N} \sum_{n=0}^{N-1} r[n] s^*[n - \tau_f \pmod{N}] e^{-j \frac{2\pi}{N} \Delta_f n} \right| \quad (41)$$

$$\tau^* = \arg \max_{\substack{\tau_f \in \{0, 1, \dots, N-1\} \\ \Delta_f \in \mathcal{D}_H}} \rho(\tau_f, \Delta_f) \quad (42)$$

We assume that the frequency offset is a uniform random variable $f_o/f_{SCS} \in [-1, 1]$ and evaluate P_{md} with $H = 3, 5$ or 7 hypotheses, wherein $\mathcal{D}_3 = \{-2/3, 0, 2/3\}$, $\mathcal{D}_5 = \{-4/5, -2/5, 0, 2/5, 4/5\}$ and $\mathcal{D}_7 = \{-6/7, -4/7, -2/7, 0, 2/7, 4/7, 6/7\}$. The number of hypotheses is a trade off between the ability to cancel the frequency offset f_o and an increase in more false timing candidates. The required SNR to obtain $P_{md} = 10^{-4}$ is contained in Table III, which shows that with a velocity of 100 km/h, all schemes perform similarly and there is no gain of using more than 3 hypotheses. With larger velocity, CCDT shows a slight gain and using more hypotheses is better.

B. Target Detection

To evaluate the radar detection ability, we assume a time discrete channel model (cf. [46]) for receiving reflections from

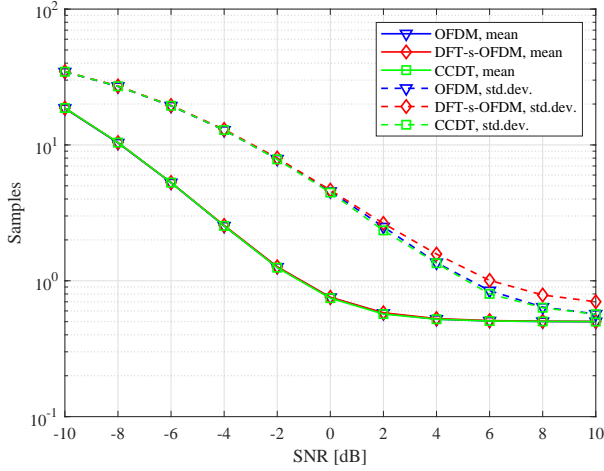


Fig. 9. Mean and standard deviation of the detected time delay τ^* using an m-sequence of length $N = 127$ at $\text{SNR}=20$ dB and 500 km/h on a Vehicular A channel, for subcarrier spacing $f_{\text{SCS}} = 15$ kHz, carrier frequency $f_c = 6$ GHz, for the waveforms OFDM, DFT-s-OFDM and CCDT with $\alpha = -2$ and $\beta = -2$.

L single point targets

$$h[n] = \sum_{l=0}^{L-1} \sqrt{\mathcal{P}_l} e^{j\phi_l} e^{j\frac{2\pi}{N}\Delta_l n} \delta[n - \tau_l] \quad (43)$$

where \mathcal{P}_l are the relative target received powers, ϕ_l comprises phase rotations which are uniformly distributed over $[-\pi, \pi)$, τ_l are the round-trip time delays of the reflected targets and Δ_l are the Doppler shifts experienced at the receiver due to the motion of the targets. The target speed v_l and range d_l can be determined by $v_l = \frac{f_{\text{SCS}}\Delta_l c}{2f_c}$ and $d_l = \frac{\tau_l c}{2Nf_{\text{SCS}}}$. We define the set $\mathcal{P} = \{\mathcal{P}_0, \mathcal{P}_1, \dots, \mathcal{P}_{L-1}\}$, assume that $\mathcal{P}_0 \geq \mathcal{P}_1 \geq \dots \geq \mathcal{P}_{L-1}$ and that the delays are uniformly distributed from the set $\tau_l \in \{0, 1, \dots, N_{\text{CP}}\}$. The Doppler shift is a continuous random uniform variable with $\Delta_l \in [-1, 1]$, i.e., it corresponds to frequencies limited by $\pm f_{\text{SCS}}$. After removing the CP, the received signal can be described as

$$r[n] = \sum_{l=0}^{L-1} \sqrt{\mathcal{P}_l} e^{j\phi_l} e^{j\frac{2\pi}{N}\Delta_l n} s[n - \tau_l \pmod{N}] + w[n]. \quad (44)$$

The objective is to estimate the delay τ^* and Doppler shift Δ^* for the strongest target, i.e., the other targets are undesired clutter in this respect. Estimation is made by computing a correlation function that is tightly related to the AF. It is evaluated on a 2-D grid of delays and Doppler shifts, which is a common practise [20], [46]. Here, the search over Doppler shifts is limited to the set $\mathcal{D}_N = \{-(N-1)/N, -(N-3)/N, \dots, (N-1)/N\}$.

$$\rho(\Delta, \tau) = \left| \frac{1}{N} \sum_{n=0}^{N-1} r[n] s^*[n - \tau \pmod{N}] e^{-j\frac{2\pi}{N}\Delta n} \right| \quad (45)$$

$$(\Delta^*, \tau^*) = \arg \max_{\substack{\tau \in \{0, 1, \dots, N_{\text{CP}}\} \\ \Delta \in \mathcal{D}_N}} \rho(\Delta, \tau) \quad (46)$$

The CP length is set to $N_{\text{CP}} = 12$ samples. We evaluate two cases: single target ($L = 1$) and multiple targets ($L =$

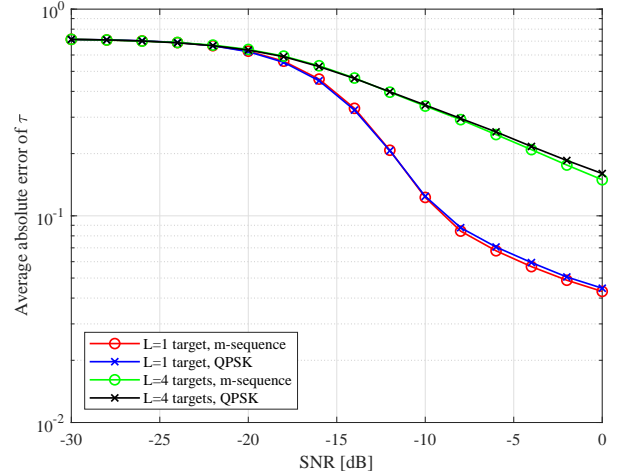


Fig. 10. Average absolute timing error for different number of targets $L = 1$ and $L = 4$, $P_{fa} = 0.01$, using QPSK or an m-sequence of length $N = 127$ for CCDT with $\alpha = -2$ and $\beta = -2$.

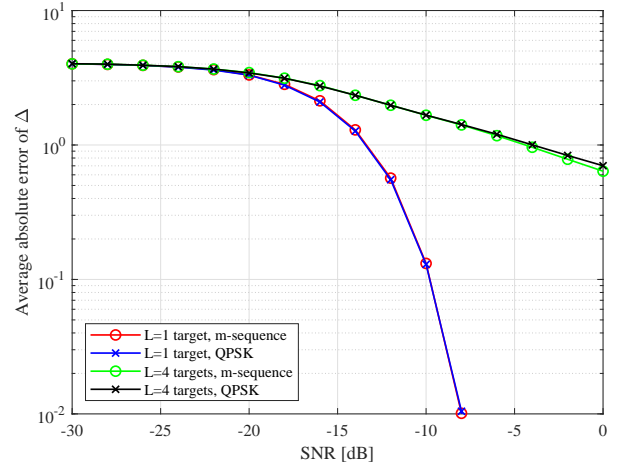


Fig. 11. Average absolute Doppler shift error for different number of targets $L = 1$ and $L = 4$, $P_{fa} = 0.01$, using QPSK or an m-sequence of length $N = 127$ for CCDT with $\alpha = -2$ and $\beta = -2$.

4) with $\mathcal{P} = \{1, 0.75, 0.5, 0.25\}$. A detection threshold, Γ , is determined to control the probability of false alarm, P_{fa} , such that $\Pr[\rho(\Delta, \tau) \geq \Gamma] \leq P_{fa}$ when the received signal is noise only, $r[n] = w[n]$. We evaluate by Monte Carlo simulations the average absolute errors for the strongest target, $|\tau^* - \tau_0|$ and $|\Delta^* - \Delta_0|$. Conversion to errors for d_0 and v_0 can be made as described above for given parameters of f_{SCS} and f_c . For transmit sequences, we use an m-sequence and a random sequence of QPSK symbols, respectively. As anticipated from Sec. II-E, both type of sequences exhibit a thumbtack-like AF and the correlation properties are expected to be similar. That is confirmed by Fig. 10 and Fig. 11, which shows that m-sequence is only slightly better than a random QPSK sequence for the case with multiple targets.

VI. CONCLUSIONS

In comparison to OFDM and DFT-s-OFDM, CCDT has the advantage that it includes tunable parameters. It was previously shown that, by proper selection of the chirp rate, CCDT could offer lower bit error rate than OFDM and DFT-s-OFDM on channels with large Doppler spread. Herein, it was found that the multicarrier chirp signal also has gains in detection performance when used as a waveform for synchronization- or radar. Moreover, selection of chirp rate and transmit sequence can flexibly shape the AF. This includes either thumbtack-like or ridge-like shapes, which are suitable for different applications, e.g., time- or frequency synchronization, or target detection. In particular, using random data as transmit sequence produces thumb-tack like shape, making the waveform suitable for JRC systems. Further study includes evaluating other types of transmit sequences than analyzed herein.

APPENDIX A PROOFS FOR PROPERTY 1 - 3

A. Lemmas

Lemma 1. For given N, Δ and τ , and $2\alpha k_m = -\Delta + (m-\tau)2\alpha + r_m N$, where $m \in \{0, 1, \dots, N-1\}$ and $k_m \in \{0, 1, \dots, N-1\}$, then

$$r_m = \begin{cases} r_0, & \text{if } m < A \\ r_0 - 2\alpha, & \text{if } m \geq A \end{cases}$$

where

$$\begin{aligned} A &= N - k_0 \\ 2\alpha k_0 &\equiv -\Delta - 2\alpha\tau \pmod{N} \\ r_0 &= \frac{2\alpha k_0 + \Delta + 2\alpha\tau}{N} \end{aligned}$$

Proof. From (56), it follows that

$$k_{m+1} \equiv k_m + 1 \pmod{N} \quad (47)$$

since

$$\begin{aligned} 2\alpha k_{m+1} &= -\Delta + 2\alpha(m+1) - 2\alpha\tau \pmod{N} \\ &= 2\alpha k_m + 2\alpha \pmod{N}. \end{aligned} \quad (48)$$

From (47), the elements of the sequence k_m belong to the set $k_m \in \{0, 1, \dots, N-1\}$ and can be expressed as

$$k_{m+1} = \begin{cases} k_m + 1, & \text{if } k_m + 1 < N \\ k_m + 1 - N, & \text{if } k_m + 1 = N. \end{cases} \quad (49)$$

The case $k_m + 1 = N$ will occur for a single value of $m = A-1$, because then $k_{m+1} \equiv 0 \pmod{N}$, and 0 appears only once in the sequence k_m . Let us assume that A is a positive integer such that $A = N - k_0$, where k_0 satisfies (56) as

$$2\alpha k_0 = -\Delta - 2\alpha\tau \pmod{N}. \quad (50)$$

Then from (56), (50) and using $2\alpha N \pmod{N} = 0$ since $2\alpha \in \mathbb{Z}$ [10], we have

$$\begin{aligned} 2\alpha k_A &\equiv -\Delta + (A-\tau)2\alpha \pmod{N} \\ &\equiv -\Delta - \tau 2\alpha - k_0 2\alpha \pmod{N} \\ &\equiv -\Delta - \tau 2\alpha - (-\Delta - \tau 2\alpha) \pmod{N} \\ &\equiv 0 \end{aligned}$$

and thus rewrite (49) as

$$k_{m+1} = \begin{cases} k_m + 1, & \text{if } m \neq A-1 \\ k_m + 1 - N, & \text{if } m = A-1. \end{cases} \quad (51)$$

The corresponding values can be obtained by inserting the values of k_{m+1} from (51) into (56). Thus, for $m \neq A-1$ we obtain $r_{m+1} = r_m$ and for $m = A-1$ it follows that $r_{m+1} = r_m - 2\alpha$. Since $2\alpha \in \mathbb{Z}$, it follows that $r_{m+1} \in \mathbb{Z}$. Hence, we have

$$\begin{aligned} r_0 &= r_1 = \dots = r_{A-1} \\ r_{N-1} &= r_{N-2} = \dots = r_A = r_{A-1} - 2\alpha \end{aligned}$$

and obtain

$$r_m = \begin{cases} r_0, & \text{if } m < A-1 \\ r_0 - 2\alpha, & \text{if } m \geq A-1. \end{cases} \quad (52)$$

Using (57), it follows that

$$r_0 = \frac{2\alpha k_0 + \Delta + 2\alpha\tau}{N}. \quad \square$$

Lemma 2. For any $0 \leq m \leq N-1$ and integer Δ , $e^{j\pi \frac{\Delta r_m}{\alpha}} = e^{j\pi \frac{\Delta r}{\alpha}}$, for any r in the set $r \in \{r_0, r_1, \dots, r_{N-1}\}$.

Proof. From Lemma 1, it follows that there are at most two different values of r_m , i.e., $r_m = r_0$ or $r_m = r_0 - 2\alpha$. Since $e^{j\pi \frac{\Delta(r_0-2\alpha)}{\alpha}} = e^{j\pi \frac{\Delta r_0}{\alpha}}$, the Lemma follows. \square

Lemma 3. For any $0 \leq m \leq N-1$, $e^{-j\frac{2\pi}{N} \left(\frac{r_m^2 N^2}{4\alpha} - \beta \frac{r_m N}{2\alpha} \right)} = e^{-j\frac{2\pi}{N} \left(\frac{r_0^2 N^2}{4\alpha} - \beta \frac{r_0 N}{2\alpha} \right)}$.

Proof. From Lemma 1, it follows that there are at most two different values of r_m , i.e., $r_m = r_0$ or $r_m = r_0 - 2\alpha$. Thus, if $r_m = r_0 - 2\alpha$ we have

$$\begin{aligned} e^{-j\frac{2\pi}{N} \left(\frac{r_m^2 N^2}{4\alpha} - \beta \frac{r_m N}{2\alpha} \right)} &= e^{-j\frac{2\pi}{N} \left(\frac{(r_0-2\alpha)^2 N^2}{4\alpha} - \beta \frac{(r_0-2\alpha) N}{2\alpha} \right)} \\ &= e^{-j\frac{2\pi}{N} \left(\frac{r_0^2 N^2}{4\alpha} - \beta \frac{r_0 N}{2\alpha} \right)} e^{j2\pi r_0 N} e^{-j2\pi(\alpha N + \beta)} \\ &= e^{-j\frac{2\pi}{N} \left(\frac{r_0^2 N^2}{4\alpha} - \beta \frac{r_0 N}{2\alpha} \right)} \end{aligned} \quad (53)$$

where the last step follows from (5). \square

B. Proof of Property 1

Inserting (2) in (9) and utilizing that (5) makes (3) to have a period N [10], i.e., $g[k] = g[k \pmod{N}]$, we obtain

$$\begin{aligned} \chi(\Delta, \tau) &= \frac{1}{N} \sum_{n=0}^{N-1} \sum_{m=0}^{N-1} \sum_{k=0}^{N-1} x[k] g[n-k] \\ &\quad \times x^*[m] g^*[n+\tau-m] e^{j\frac{2\pi}{N} \Delta n} \\ &= \sum_{m=0}^{N-1} \sum_{k=0}^{N-1} x[k] x^*[m] e^{-j\frac{2\pi}{N} (\alpha(k^2 - m^2) + \beta(m-k) + 2\alpha\tau m)} \\ &\quad \times C_0 \sum_{n=0}^{N-1} e^{j\frac{2\pi}{N} n(\Delta - 2\alpha(m-k) + 2\alpha\tau)}. \end{aligned} \quad (54)$$

with $C_0 = \frac{g^*[\tau]e^{-j\frac{2\pi}{N}\tau\gamma}}{N\sqrt{N}}$. A well-known identity is that for $k \in \mathbb{Z}$:

$$\sum_{n=0}^{N-1} e^{j\frac{2\pi}{N}nk} = N\delta[k \pmod{N}] \quad (55)$$

Therefore, the inner sum in (54) is non-zero and equal to N only when there for each m exists a $k = k_m$ and $k \in \{0, 1, \dots, N-1\}$ such that

$$2\alpha k_m \equiv -\Delta + (m - \tau)2\alpha \pmod{N}. \quad (56)$$

The condition (56) is a linear congruence equation having only a single k_m as solution for each m due to (4). We can rewrite (56) as

$$2\alpha k_m = -\Delta + (m - \tau)2\alpha + r_m N \quad (57)$$

where $r_m \in \mathbb{Z}$. Inserting k_m from (57) in (54) gives

$$\begin{aligned} \chi(\Delta, \tau) &= C_1 \sum_{m=0}^{N-1} x \left[m - \tau + \frac{r_m N - \Delta}{2\alpha} \right] x^*[m] \\ &\quad \times e^{-j\frac{2\pi}{N} \left(\frac{r_m^2 N^2}{4\alpha} - \beta \frac{r_m N}{2\alpha} \right)} e^{j\pi \frac{\Delta r_m}{\alpha}} e^{j\frac{2\pi}{N} \Delta m} \\ &\stackrel{(a)}{=} C \sum_{m=0}^{N-1} x \left[m - \tau + \frac{r_m N - \Delta}{2\alpha} \right] x^*[m] e^{j\frac{2\pi}{N} \Delta m} \\ &\stackrel{(b)}{=} C \sum_{m=0}^{N-1} x \left[m - \tau + \frac{r_0 N - \Delta}{2\alpha} \pmod{N} \right] x^*[m] \\ &\quad \times e^{j\frac{2\pi}{N} \Delta m} \end{aligned} \quad (58)$$

with $C_1 = C_0 \sqrt{N} e^{j\frac{2\pi}{N}\tau\gamma} g^*[\tau + \Delta/2\alpha]$ and $C = C_1 N \sqrt{N} e^{j\frac{2\pi}{N}\tau\gamma} g^*[-r_0 N/2\alpha] e^{j\pi \frac{\Delta r_0}{\alpha}}$, where replacing r_m with $r_m = r_0$ and moving the exponential terms outside the sum in (a) follows from Lemma 2 and Lemma 3 in Appendix A. Replacing r_m with $r_m = r_0$ or $r_m = r_0 - 2\alpha$ in the sequence argument in (b) follows from Lemma 1, and since 2α is an integer [10] and $-2\alpha N \equiv 0 \pmod{N}$, the modulo- N operator is introduced.

C. Proof of Property 2

The condition $\Delta + 2\alpha\tau \equiv 0 \pmod{N}$ is equivalent to $\Delta + 2\alpha\tau = rN$ with $r \in \mathbb{Z}$, which is obtained from (57) by using $k_m = m$ and $r_m = r$. Therefore, $(r_m N - \Delta)/2\alpha = \tau$ and from (10), utilizing $|C| = 1/N$ and (55) we have

$$|\chi(\Delta, \tau)| = \frac{1}{N} \left| \sum_{m=0}^{N-1} x[m] x^*[m] e^{j\frac{2\pi}{N} \Delta m} \right| = \begin{cases} 0, & \Delta \neq 0 \\ 1, & \Delta = 0. \end{cases}$$

It follows from (4) that if $\Delta + 2\alpha\tau \equiv 0 \pmod{N}$ and $\Delta = 0$, then $\tau = 0$, i.e., the AF is $|\chi(\Delta, \tau)| = \delta[\Delta]$.

D. Proof of Property 3

Let us define $\epsilon(\tau) = -\tau + (r_0 N - \Delta)/2\alpha$ and insert $x[m]$ in (10) to obtain

$$\begin{aligned} \sum_{\tau=0}^{N-1} |\chi(\Delta, \tau)|^2 &= \sum_{\tau=0}^{N-1} \chi(\Delta, \tau) \chi^*(\Delta, \tau) \\ &\stackrel{(a)}{=} \frac{1}{N^2} \sum_{\tau=0}^{N-1} \sum_{n=0}^{N-1} x[n] x^*[n + \epsilon(\tau)] e^{j\frac{2\pi}{N} \Delta n} \\ &\quad \times \sum_{m=0}^{N-1} x^*[m] x[m + \epsilon(\tau)] e^{-j\frac{2\pi}{N} \Delta m} \\ &\stackrel{(b)}{=} \frac{1}{N^2} \sum_{n=0}^{N-1} \sum_{m=0}^{N-1} x[n] x^*[m] e^{j\frac{2\pi}{N} \Delta(n-m)} \\ &\quad \times \sum_{\tau=0}^{N-1} x^*[n + \epsilon(\tau)] x[m + \epsilon(\tau)] \\ &\stackrel{(c)}{=} \frac{1}{N^2} \sum_{n=0}^{N-1} \sum_{m=0}^{N-1} x[n] x^*[m] e^{j\frac{2\pi}{N} \Delta(n-m)} \\ &\quad \times N\delta[n - m] \\ &\stackrel{(d)}{=} \frac{1}{N} \sum_{n=0}^{N-1} x[n] x^*[n] \\ &\stackrel{(e)}{=} 1 \end{aligned}$$

where (a)-(b) follow by definition, (c) is due to (17) and (d)-(e) are due to (16), and all additions of sequence indices in $x[m]$ are performed \pmod{N} .

APPENDIX B PROOFS FOR PROPERTY 4 - 6

A. Proof for Property 4

By insertion of $x_k[m]$ in (10) and (55)

$$\begin{aligned} |\chi(\Delta, \tau)| &= \frac{1}{N} \left| \sum_{m=0}^{N-1} e^{j\frac{2\pi}{N} \frac{kr_m N}{2\alpha}} e^{j\frac{2\pi}{N} \Delta m} \right| \\ &= \frac{1}{N} \left| \sum_{m=0}^{N-1} e^{j\frac{2\pi}{N} \Delta m} \right| = \begin{cases} 0, & \Delta \neq 0 \\ 1, & \Delta = 0. \end{cases} \end{aligned}$$

where it follows from Lemma 1 in Appendix A, that $e^{j\frac{2\pi}{N} \frac{kr_m N}{2\alpha}} = e^{j\frac{2\pi}{N} \frac{kr_0 N}{2\alpha}}$, because there are at most two different values of r_m , i.e., r_0 or $r_0 - 2\alpha$, and $e^{j\frac{2\pi}{N} \frac{k(r_0 - 2\alpha)N}{2\alpha}} = e^{j\frac{2\pi}{N} \frac{kr_0 N}{2\alpha}}$.

B. Proof for Property 5

Let us define $\epsilon = -\tau + (r_0 N - \Delta)/2\alpha$ and insert $x_u[m]$ in (10) to obtain

$$|\chi(\Delta, \tau)| = \frac{1}{N} \left| \sum_{m=0}^{N-1} e^{j\frac{2\pi}{N} m(\Delta + u\epsilon)} \right| \quad (59)$$

where we have used $x_u[m + \epsilon \pmod{N}] = x_u[m + \epsilon]$. The modulus AF (59) is equal to 1 when

$$\Delta + u \left(-\tau + \frac{r_0 N - \Delta}{2\alpha} \right) \equiv 0 \pmod{N}$$

which can be simplified as

$$2\alpha\Delta - u(2\alpha\tau + \Delta) \equiv 0 \pmod{N}. \quad (60)$$

When $u = 2\alpha$ and $\tau = 0$, (60) holds for all Δ , i.e., $|\chi(\Delta, \tau = 0)| = 1$. When $u = 2\alpha$, $\tau \neq 0$ and $\Delta \neq 0$, we have $2\alpha\Delta - 2\alpha(2\alpha\tau + \Delta) = -4\alpha^2\tau$ and due to (4) and that τ is an integer, it follows that $-4\alpha^2\tau \not\equiv 0 \pmod{N}$, and thus, $|\chi(\Delta \neq 0, \tau \neq 0)| = 0$.

C. Proof for Property 6

Lemma 4 If $x[m]$ is an m-sequence and $0 < \tau \leq N - 1$, then $x[m]x[m + \tau \pmod{N}] = -x[m + \tau' \pmod{N}]$ for some τ' .

Proof. Let $y[m]$ be a binary m-sequence and $x[m] = q[y[m]]$ with

$$q[b] = \begin{cases} -1, & b = 0 \\ 1, & b = 1. \end{cases} \quad (61)$$

It is straightforward to verify that for $b_0 \in \{0, 1\}$ and $b_1 \in \{0, 1\}$:

$$q(b_0 + b_1 \pmod{2}) = -q(b_0)q(b_1) \quad (62)$$

The shift-and-add property of m-sequences gives that $y[m + \tau \pmod{N} + y[m] \pmod{2}] = y[m + \tau' \pmod{N}]$ for $0 < \tau \leq N - 1$, $m = 0, 1, \dots, N - 1$, where τ' depends on τ . Therefore, applying (62) to this identity results in $x[m]x[m + \tau \pmod{N}] = -x[m + \tau' \pmod{N}]$. \square

Lemma 5. If $x[m]$ is an m-sequence and $|\chi(\Delta \neq 0, \tau_0)| \neq 0$ and if $\Delta + 2\alpha\tau_1 \not\equiv 0 \pmod{N}$, then $|\chi(\Delta \neq 0, \tau_1)| = |\chi(\Delta \neq 0, \tau_0)|$ for $\tau_0 \neq \tau_1$.

Proof. Let us define $\epsilon(\tau) = -\tau + (r_0N - \Delta)/2\alpha$. From (57), by using $k_m = m$ there exists an r_m such that $\Delta = -2\alpha\tau + rN$, thus $\epsilon(\tau) \not\equiv 0 \pmod{N}$. Consequently, if $\Delta + 2\alpha\tau \not\equiv 0 \pmod{N}$, then $\epsilon(\tau) \not\equiv 0 \pmod{N}$. Assume that $|\chi(\Delta \neq 0, \tau_0)| \neq 0$ and an integer t such that

$$\begin{aligned} |\chi(\Delta \neq 0, \tau_0)| &= \frac{1}{N} \left| \sum_{m=0}^{N-1} x[m + \epsilon(\tau_0) \pmod{N}] x[m] e^{j\frac{2\pi}{N}\Delta m} \right| \\ &\stackrel{(a)}{=} \frac{1}{N} \left| \sum_{m=0}^{N-1} x[m + \tau' \pmod{N}] e^{j\frac{2\pi}{N}\Delta m} \right| \\ &\stackrel{(b)}{=} \frac{1}{N} \left| \sum_{m=t}^{N-1+t} x[m + \tau' - t \pmod{N}] \right. \\ &\quad \left. \times e^{j\frac{2\pi}{N}\Delta(m-t)} \right| \\ &\stackrel{(c)}{=} \frac{1}{N} \left| \sum_{m=0}^{N-1} x[m + \tau' - t \pmod{N}] e^{j\frac{2\pi}{N}\Delta(m-t)} \right| \\ &\stackrel{(d)}{=} \frac{1}{N} \left| \sum_{m=0}^{N-1} x[m + \tau_1 \pmod{N}] x^*[m] \right. \\ &\quad \left. \times e^{j\frac{2\pi}{N}\Delta(m-t)} \right| \\ &\stackrel{(e)}{=} |\chi(\Delta \neq 0, \tau_1) e^{-j\frac{2\pi}{N}\Delta t}| \\ &\stackrel{(f)}{=} |\chi(\Delta \neq 0, \tau_1)| \end{aligned}$$

where Lemma 4 was used in (a) and (d) and the change of summation index from (b) to (c) follows from the periodicity in N of the exponential function and the sequence $x[m]$. \square

Lemma 6. If $x[m]$ is an m-sequence, then

$$\sum_{\tau=0}^{N-1} |\chi(\Delta, \tau)|^2 = \begin{cases} 1 + (N-1)\frac{1}{N^2}, & \Delta = 0 \\ 1 - \frac{1}{N^2}, & \Delta \neq 0. \end{cases}$$

Proof. Let us define $\epsilon(\tau) = -\tau + (r_0N - \Delta)/2\alpha$ and insert $x[m]$ in (10) to obtain

$$\begin{aligned} \sum_{\tau=0}^{N-1} |\chi(\Delta, \tau)|^2 &= \sum_{\tau=0}^{N-1} \chi(\Delta, \tau) \chi^*(\Delta, \tau) \\ &= \frac{1}{N^2} \sum_{\tau=0}^{N-1} \sum_{n=0}^{N-1} x[n] x[n + \epsilon(\tau)] e^{j\frac{2\pi}{N}\Delta n} \\ &\quad \times \sum_{m=0}^{N-1} x[m] x[m + \epsilon(\tau)] e^{-j\frac{2\pi}{N}\Delta m} \\ &= \frac{1}{N^2} \sum_{n=0}^{N-1} \sum_{m=0}^{N-1} x[n] x[m] e^{j\frac{2\pi}{N}\Delta(n-m)} \\ &\quad \times \sum_{\tau=0}^{N-1} x[n + \epsilon(\tau)] x[m + \epsilon(\tau)] \\ &= \frac{1}{N^2} \sum_{n=0}^{N-1} \sum_{m=0}^{N-1} x[n] x[m] e^{j\frac{2\pi}{N}\Delta(n-m)} \\ &\quad \times N\rho(n-m) \\ &= \frac{1}{N} \sum_{t=0}^{N-1} \sum_{m=0}^{N-1} x[m+t] x[m] e^{j\frac{2\pi}{N}\Delta t} \rho(t) \\ &= \sum_{t=0}^{N-1} \rho^2(t) e^{j\frac{2\pi}{N}\Delta t} \end{aligned}$$

where all additions of sequence indices are performed \pmod{N} and where the change to summation index t follows from the periodicity in N of the exponential function and the periodicity of the sequence $x[m \pmod{N}]$. If $\Delta = 0$, then $\sum_{t=0}^{N-1} \rho^2(t) e^{j\frac{2\pi}{N}\Delta t} = 1 + (N-1)\frac{1}{N^2}$. If $\Delta \neq 0 \pmod{N}$, then

$$\begin{aligned} \sum_{t=0}^{N-1} \rho^2(t) e^{j\frac{2\pi}{N}\Delta t} &= \rho^2(0) + \sum_{t=1}^{N-1} \rho^2(t) e^{j\frac{2\pi}{N}\Delta t} \\ &= 1 + \frac{1}{N^2} \left(\sum_{t=0}^{N-1} e^{j\frac{2\pi}{N}\Delta t} - \rho^2(0) \right) \\ &= 1 + \frac{1}{N^2} (0 - 1) \\ &= 1 - \frac{1}{N^2}. \end{aligned}$$

Thus,

$$\sum_{\tau=0}^{N-1} |\chi(\Delta, \tau)|^2 = \begin{cases} 1 + (N-1)\frac{1}{N^2}, & \Delta = 0 \\ 1 - \frac{1}{N^2}, & \Delta \neq 0. \end{cases} \quad \square$$

Property 6 can then be proved as follows. The first case is trivial and case two and three follow straightforwardly from (18) and Property 2, respectively. The fourth case is proved as follows. For a given $\Delta \neq 0$, Property 2 gives that there exists one τ ($\tau \in \{0, 1, \dots, N-1\}$) for which $|\chi(\Delta \neq 0, \tau)| = 0$, since the linear congruence equation $\Delta + 2\alpha\tau \equiv 0 \pmod{N}$ has one solution τ when (4) holds. Thus, are $N-1$ values of τ where $|\chi(\Delta \neq 0, \tau)| \neq 0$. From Lemma 5 and Lemma 6 in

Appendix B, we then have $(N-1)|\chi(\Delta \neq 0, \tau)|^2 = 1 - 1/N^2$ and we can solve for $|\chi(\Delta \neq 0, \tau)| = \sqrt{(N+1)/N}$.

APPENDIX C AMBIGUITY FUNCTION WITH UPSAMPLING

Consider (6) with upsampling such that $(Q/N) \in \mathbb{Z}$ and

$$s[n] = \frac{1}{\sqrt{Q}} \sum_{m=0}^{N-1} G[m]X[m]e^{j\frac{2\pi}{Q}mn} \quad (63)$$

for $n = 0, 1, \dots, Q-1$. Using (63), (7) and (8), we obtain

$$\begin{aligned} \chi(\Delta, \tau) &= \frac{1}{Q} \sum_{n=0}^{Q-1} s[n]s^*[n + \tau \pmod{Q}]e^{j\frac{2\pi}{Q}\Delta n} \\ &= \frac{1}{Q^2} \sum_{m=0}^{N-1} \sum_{p=0}^{N-1} G[m]X[m]G^*[p]X^*[p]e^{-j\frac{2\pi}{Q}p\tau} \\ &\quad \times \sum_{n=0}^{Q-1} e^{j\frac{2\pi}{Q}n(m-p+\Delta)} \end{aligned} \quad (64)$$

which holds for arbitrary Δ . For non-integer Δ , the inner sum in (64) can be replaced by:

$$\sum_{n=0}^{Q-1} e^{j\frac{2\pi}{Q}n(m-p+\Delta)} = \frac{\sin(\pi(m-p+\Delta))}{\sin\left(\frac{\pi(m-p+\Delta)}{Q}\right)} \times e^{j\frac{\pi(Q-1)(m-p+\Delta)}{Q}} \quad (65)$$

For integer Δ , the inner sum can be replaced by $Q\delta[m-p+\Delta \pmod{Q}]$ and we can proceed from (64) by

$$\begin{aligned} \chi(\Delta, \tau) &= \frac{1}{Q} \sum_{p=0}^{N-1} G[p-\Delta+r_pQ]X[p-\Delta+r_pQ] \\ &\quad \times G^*[p]X^*[p]e^{-j\frac{2\pi}{Q}p\tau} \end{aligned} \quad (66)$$

where $r_p \in \mathbb{Z}$. Furthermore, using (7) and (8), it follows that

$$\begin{aligned} G[p-\Delta+r_pQ]G^*[p] &= \sum_{k=0}^{N-1} g[k]e^{-j\frac{2\pi}{N}(p-\Delta+r_pQ)k} \\ &\quad \times \sum_{t=0}^{N-1} g^*[t]e^{j\frac{2\pi}{N}pt} \\ &= \sum_{v=0}^{N-1} \sum_{k=0}^{N-1} g[k]g^*[k+v] \\ &\quad \times e^{j\frac{2\pi}{N}pv}e^{j\frac{2\pi}{N}\Delta k} \\ &= N \sum_{v=0}^{N-1} \chi_g(\Delta, v)e^{j\frac{2\pi}{N}pv} \end{aligned} \quad (67)$$

and similarly

$$\begin{aligned} X[p-\Delta+r_pQ]X^*[p] &= \frac{1}{N} \sum_{k=0}^{N-1} x[k]e^{-j\frac{2\pi}{N}(p-\Delta+r_pQ)k} \\ &\quad \times \sum_{t=0}^{N-1} x^*[t]e^{j\frac{2\pi}{N}pt} \\ &= \sum_{w=0}^{N-1} \chi_x(\Delta, w)e^{j\frac{2\pi}{N}pw}. \end{aligned} \quad (68)$$

Therefore, by using (25), (66) can be written as:

$$\begin{aligned} \chi(\Delta, \tau) &= \frac{N}{Q} \sum_{v=0}^{N-1} \chi_g(\Delta, v) \sum_{w=0}^{N-1} \chi_x(\Delta, w) \\ &\quad \times \sum_{p=0}^{N-1} e^{j\frac{2\pi}{N}p(v+w-\frac{N}{Q}\tau)} \\ &= \frac{N}{Q} \sum_{v=0}^{N-1} \sum_{w=0}^{N-1} \chi_g(\Delta, v)\chi_x(\Delta, w) \\ &\quad \times \frac{\sin\left(\pi\left(v+w-\frac{N}{Q}\tau\right)\right)}{\sin\left(\frac{\pi\left(v+w-\frac{N}{Q}\tau\right)}{N}\right)} e^{j\frac{\pi(N-1)\left(v+w-\frac{N}{Q}\tau\right)}{N}}. \end{aligned} \quad (69)$$

For the special case of $Q = N$, i.e., no upsampling, (55) can be used to give $N\delta[v+w-\tau \pmod{N}]$ for the inner sum in (69) such that

$$\chi(\Delta, \tau) = N \sum_{v=0}^{N-1} \chi_g(\Delta, v)\chi_x(\Delta, \tau-v). \quad (71)$$

APPENDIX D ALTERNATIVE DERIVATION OF PROPERTY 1

By using (3), it follows that

$$\begin{aligned} \chi_g(\Delta, \tau) &= \frac{1}{N} \sum_{n=0}^{N-1} g[n]g^*[n + \tau \pmod{N}]e^{j\frac{2\pi}{N}\Delta n} \\ &= \frac{1}{N^2} e^{j\frac{2\pi}{N}(\alpha\tau^2+\beta\tau)} \sum_{n=0}^{N-1} e^{j\frac{2\pi}{N}(2\alpha\tau+\Delta)n} \\ &= \frac{1}{N} e^{j\frac{2\pi}{N}(\alpha\tau^2+\beta\tau)} \delta[2\alpha\tau + \Delta \pmod{N}]. \end{aligned} \quad (72)$$

Furthermore, by definition it follows that

$$\begin{aligned} \chi_x(\Delta, \tau) &= \frac{1}{N} \sum_{n=0}^{N-1} x[n]x^*[n + \tau \pmod{N}]e^{j\frac{2\pi}{N}\Delta n} \\ &= \frac{1}{N} \sum_{n=0}^{N-1} x[n-\tau \pmod{N}]x^*[n]e^{j\frac{2\pi}{N}\Delta(n-\tau)}. \end{aligned} \quad (73)$$

Let $r \in \mathbb{Z}$ be a solution to $2\alpha v + \Delta = rN$. Due to (4), there exists one unique r when $v = 0, 1, \dots, N-1$. Thus, (73) is non-zero only when $v = (rN - \Delta)/2\alpha$. The modulus AF is obtained from (24) with (72) and (73) as

$$\begin{aligned} |\chi(\Delta, \tau)| &= \left| \sum_{v=0}^{N-1} \delta[2\alpha v + \Delta \pmod{N}] \right. \\ &\quad \times \frac{1}{N} \sum_{n=0}^{N-1} x[n-\tau+v \pmod{N}]x^*[n]e^{j\frac{2\pi}{N}\Delta(n-\tau+v)} \left. \right| \\ &= \left| \frac{1}{N} \sum_{n=0}^{N-1} x\left[n-\tau + \left(\frac{rN-\Delta}{2\alpha}\right) \pmod{N}\right] \right. \\ &\quad \times x^*[n]e^{j\frac{2\pi}{N}\Delta n} \left. \right|. \end{aligned} \quad (74)$$

APPENDIX E
PROOFS FOR PROPERTY 7 - 12

A. Proof for Property 7

By insertion of $x[m]$ in (28) and using (55)

$$|\chi(\Delta = 0, \tau)| = \frac{1}{N} \left| \sum_{m=0}^{N-1} x[m] x^*[m] e^{-j \frac{2\pi}{N} \tau m} \right| = \begin{cases} 0, & \tau \neq 0 \\ 1, & \tau = 0. \end{cases}$$

B. Proof for Property 8

By insertion of $x_k[m]$ in (28) and (55)

$$|\chi(\Delta, \tau)| = \frac{1}{N} \left| \sum_{m=0}^{N-1} e^{-j \frac{2\pi}{N} \tau m} \right| = \begin{cases} 0, & \tau \neq 0 \\ 1, & \tau = 0. \end{cases} \quad (75)$$

C. Proof for Property 9

By insertion of $x_u[m]$ in (28) and (55)

$$\begin{aligned} |\chi(\Delta, \tau)| &= \frac{1}{N} \left| \sum_{k=0}^{N-1} \sum_{m=0}^{N-1} e^{j \frac{2\pi}{N} u k(k+1)} e^{-j \frac{2\pi}{N} u m(m+1)} e^{-j \frac{2\pi}{N} \tau m} \right. \\ &\quad \left. \times \sum_{n=0}^{N-1} e^{j \frac{2\pi}{N} n(k-m+\Delta)} \right| \\ &\stackrel{(a)}{=} \frac{1}{N} \left| \sum_{m=0}^{N-1} e^{-j \frac{2\pi}{N} m(-u(rN-\Delta)+\tau)} \right| \\ &\stackrel{(b)}{=} \begin{cases} 0, & \tau + u\Delta \not\equiv 0 \pmod{N} \\ 1, & \tau + u\Delta \equiv 0 \pmod{N} \end{cases} \end{aligned}$$

where (a) follows from that the inner sum is $\delta[k - m + \Delta \pmod{N}]$ which gives $k = m - \Delta + rN$ for $r \in \mathbb{Z}$. Step (b) follows from that the sum is $\delta[-u(rN - \Delta) + \tau \pmod{N}] = \delta[u\Delta + \tau \pmod{N}]$.

D. Proof for Property 10

By insertion of $x_k[m]$ in (28) and using (55)

$$|\chi(\Delta, \tau = 0)| = \frac{1}{N} \left| \sum_{m=0}^{N-1} x[m] x^*[m] e^{j \frac{2\pi}{N} \Delta m} \right| = \begin{cases} 0, & \Delta \neq 0 \\ 1, & \Delta = 0. \end{cases}$$

E. Proof for Property 11

By insertion of $x_k[m]$ in (31) and using (55)

$$|\chi(\Delta = 0, \tau)| = \frac{1}{N} \left| \sum_{m=0}^{N-1} e^{j \frac{2\pi}{N} \Delta m} \right| = \begin{cases} 0, & \Delta \neq 0 \\ 1, & \Delta = 0. \end{cases}$$

F. Proof for Property 12

By insertion of $x_u[m]$ in (31) and (55)

$$\begin{aligned} |\chi(\Delta = 0, \tau)| &= \frac{1}{N} \left| \sum_{m=0}^{N-1} e^{j \frac{2\pi}{N} m(\Delta - \tau u)} \right| \quad (76) \\ &= \begin{cases} 0, & \Delta - \tau u \not\equiv 0 \pmod{N} \\ 1, & \Delta - \tau u \equiv 0 \pmod{N}. \end{cases} \quad (77) \end{aligned}$$

APPENDIX F
PROOFS FOR PROPERTY 13 - 14

A. Proof for Property 13

Case 1 ($u = 2\alpha$). Inserting $x_u[m]$ in (2) gives:

$$\begin{aligned} \text{PAPR} &= \max_{0 \leq n \leq N-1} \left| \frac{1}{\sqrt{N}} e^{-j \frac{2\pi}{N} (\alpha n^2 + \beta n + \gamma)} \sum_{m=0}^{N-1} e^{j \frac{2\pi}{N} (\alpha + 2\alpha n + \beta) m} \right|^2 \\ &= \max_{0 \leq n \leq N-1} \left| \frac{1}{\sqrt{N}} \sum_{m=0}^{N-1} e^{j \frac{2\pi}{N} (\alpha + 2\alpha n + \beta) m} \right|^2 \end{aligned}$$

If $\alpha \in \mathbb{Z}$, then it follows from (5) $\beta \in \mathbb{Z}$, therefore $\alpha + 2\alpha n + \beta \in \mathbb{Z}$, since $2\alpha \in \mathbb{Z}$. If $\alpha = p/2$ for any odd integer p , then there exists an odd integer q such that $\beta = q/2$ and $\alpha + \beta = (p+q)/2 \in \mathbb{Z}$, therefore $\alpha + 2\alpha n + \beta \in \mathbb{Z}$. Thus

$$\frac{1}{\sqrt{N}} \sum_{m=0}^{N-1} e^{j \frac{2\pi}{N} (\alpha + 2\alpha n + \beta) m} = \begin{cases} \sqrt{N}, & \alpha + 2\alpha n + \beta \equiv 0 \pmod{N} \\ 0, & \alpha + 2\alpha n + \beta \not\equiv 0 \pmod{N} \end{cases} \quad (78)$$

and we obtain $\max_{0 \leq n \leq N-1} |s[n]|^2 = N$, i.e., $\text{PAPR} = 10 \log_{10} N$.

Case 2 ($u \neq 2\alpha$). Inserting $x_u[m]$ in (2) gives:

$$\text{PAPR} = \max_{0 \leq n \leq N-1} \left| \sum_{m=0}^{N-1} e^{-j \frac{2\pi}{N} ((\alpha - \frac{u}{2}) m^2 - (\frac{u}{2} + 2\alpha n + \beta) m)} \right|^2$$

Let us define $a = \alpha - \frac{u}{2}$, $b = -(\frac{u}{2} + 2\alpha n + \beta)$ and

$$S = \left| \frac{1}{\sqrt{N}} \sum_{m=0}^{N-1} e^{-j \frac{2\pi}{N} (am^2 + bm)} \right|^2$$

then $\text{PAPR} = \max_{0 \leq n \leq N-1} S$ and

$$\begin{aligned} S &= \frac{1}{N} \sum_{m=0}^{N-1} e^{-j \frac{2\pi}{N} (am^2 + bm)} \sum_{n=0}^{N-1} e^{j \frac{2\pi}{N} (an^2 + bn)} \\ &= \frac{1}{N} \sum_{m=0}^{N-1} \sum_{n=0}^{N-1} e^{-j \frac{2\pi}{N} (m-n)(a(n+m)+b)} \\ &= \frac{1}{N} \sum_{m=0}^{N-1} \sum_{n=0}^{N-1} e^{-j \frac{2\pi}{N} ((m-n)2an - (m-n)^2 a + (m-n)b)} \\ &= \frac{1}{N} \sum_{t=0}^{N-1} \sum_{n=0}^{N-1} e^{-j \frac{2\pi}{N} (t2an - t^2 a + tb)} \\ &= \frac{1}{N} \sum_{t=0}^{N-1} \left(\sum_{n=0}^{N-1} e^{-j \frac{2\pi}{N} t2an} \right) e^{-j \frac{2\pi}{N} (-t^2 a + tb)} \\ &= \frac{1}{N} N \quad (79) \end{aligned}$$

The last step follows since $t2a = t2\alpha - tu \in \mathbb{Z}$, N is a prime, $\gcd(u, N) = 1$ and thus $\gcd(t2a, N) = 1$ and $t2\alpha \pmod{N} \neq 0$. Hence, the inner sum is equal to N when $t = 0$. Therefore, $\max_{0 \leq n \leq N-1} |s[n]|^2 = 1$ and $\text{PAPR} = 0$ dB.

The variable substitution $t = m - n$ apply in the range $0 \leq t \leq N - 1$ since

- i) $e^{-j \frac{2\pi}{N} t2an}$
- ii) $e^{-j \frac{2\pi}{N} (-t^2 a + tb)}$

have period of N . For i), it directly follows from that $t2a = t(2\alpha - u)$ is an integer. For ii), it can be shown as follows,

$$\begin{aligned} e^{-j\frac{2\pi}{N}(-(t+N)^2a+b(t+N))} &= e^{-j\frac{2\pi}{N}(-t^2a+bt)} e^{-j2\pi(-Na-2ta+b)} \\ &= e^{-j\frac{2\pi}{N}(-t^2a+bt)} e^{j2\pi(N\alpha+\beta)} \\ &\quad \times e^{j2\pi2\alpha(t+n)} e^{-j2\pi\frac{u}{2}(N+2t-1)} \\ &= e^{-j\frac{2\pi}{N}(-t^2a+bt)} \end{aligned}$$

where (5) and $2\alpha \in \mathbb{Z}$ are used, and since $\frac{u}{2}(N+2t-1) \in \mathbb{Z}$ for odd N .

B. Proof for Property 14

Inserting $x_k[m]$ in (2) gives

$$\text{PAPR} = \max_{0 \leq n \leq N-1} \left| \sum_{m=0}^{N-1} e^{-j\frac{2\pi}{N}(\alpha m^2 - (k+2\alpha n+\beta)m)} \right|^2$$

Let us define $a = \alpha$, $b = -(k+2\alpha n+\beta)$ and perform the same steps as in Case 2 of the proof of Property 13. Thus

$$S = \frac{1}{N} \sum_{t=0}^{N-1} \left(\sum_{n=0}^{N-1} e^{-j\frac{2\pi}{N}t2an} \right) e^{-j\frac{2\pi}{N}(-t^2a+tb)}$$

and it follows straightforwardly that $e^{-j2\pi(-Na-2ta+b)} = e^{-j2\pi(-N\alpha-\beta-2t\alpha-k-2\alpha n)} = 1$ due to (5), $2\alpha \in \mathbb{Z}$, and k and t being integers. Therefore, $e^{-j\frac{2\pi}{N}(-(t+N)^2a+(t+N)b)} = e^{-j\frac{2\pi}{N}(-t^2a+tb)} e^{-j2\pi(-Na-2ta+b)}$ has a period of N and the same substitution $t = m - n$ in S is applicable. Hence, $S = 1$ and PAPR = 0 dB.

REFERENCES

- [1] J. R. Klauder, A. C. Price, S. Darlington, and W. J. Albersheim, "The theory and design of chirp radars," *The Bell Sys. Tech. J.*, vol. 39, no. 4, pp. 745-808, July 1960.
- [2] A. Meta, P. Hoogetboom, and L. P. Ligthart, "Signal processing for FMCW SAR," *IEEE Trans. Geoscience Remote Sensing*, vol. 45, no. 11, pp. 3519-3532, Nov. 2007.
- [3] H. Rohling, M.-M. Meinecke, "Waveform design principles for automotive radar systems," *CIE Int. Conf. on Radar Proceedings*, Beijing, China, 2001, pp. 1-4.
- [4] M. O. Khyam, L. Xinde, S. S. Ge, and M. R. Pickering, "Multiple access chirp-based ultrasonic positioning," *IEEE Trans. Instrumentation and Measurement*, vol. 66, no. 12, pp. 3126-3137, Dec. 2017.
- [5] J. Zhang, M. M. Qang, and T. Xia, "Practical synchronization waveform for massive machine-type communications," *IEEE Trans. Commun.*, vol. 67, no. 2, pp. 1467-1479, Feb. 2019.
- [6] M. Martone, "A multicarrier system based on the fractional Fourier transform for time-frequency-selective channels," *IEEE Trans. Commun.*, vol. 49, no. 6, pp. 1011-1020, June 2001.
- [7] T. Erseghe, N. Laurenti, and V. Cellini, "A multicarrier architecture based upon the affine Fourier transform," *IEEE Trans. Commun.*, vol. 53, no. 5, pp. 853-862, May 2005.
- [8] X. Ouyang and J. Zhao, "Orthogonal chirp division multiplexing," *IEEE Trans. Commun.*, vol. 64, no. 9, pp. 3946-3957, Sept. 2016.
- [9] A. Şahin, N. Hosseini, H. Jamal, S. S. M. Hoque, and D. W. Matolak, "DFT-spread-OFDM Based Chirp Transmission," *IEEE Commun. Lett.*, vol. 25, no. 3, pp. 902-906, Mar. 2021.
- [10] F. Berggren and B. M. Popović, "Chirp-convolved data transmission," *IEEE Commun. Lett.*, vol. 25, no. 4, pp. 1226-1230, Apr. 2021.
- [11] *Solutions for NR to support non-terrestrial networks (NTN) (Release 16)*, document 3GPP TR 38.821 V16.0.0, Dec., 2019.
- [12] R. He, F. Bai, G. Mao, J. Härri, and P. Kyösti, "Guest editorial 5G wireless communications with high mobility," *IEEE J. Sel. Areas in Commun.*, vol. 38, no. 12, pp. 2717-2722, Dec. 2020.
- [13] *Study on Scenarios and Requirements for Next Generation Access Technologies; (Release 16)*, document 3GPP TR 38.913 V16.0.0, July, 2020. [Online]. Available: <https://www.3gpp.org>
- [14] C. Sturm and W. Wiesbeck, "Waveform design and signal processing aspects for fusion of wireless communications and radar sensing," *Proc. of the IEEE*, vol. 99, no. 7, pp. 1236-1259, July 2011.
- [15] B. Paul, A. R. Chiriyath, and D. W. Bliss, "Survey of RF communications and sensing convergence research," *IEEE Access*, vol. 5, pp. 252-270, 2017.
- [16] F. Liu, C. Masouros, A. P. Petropulu, H. Griffiths, and L. Hanzo, "Joint radar and communication design: applications, state-of-the-art, and the road ahead," *IEEE Trans. Commun.*, vol. 68, no. 6, pp. 3834-3862, June 2020.
- [17] S. H. Dokhanchi, B. S. Mysore, K. V. Mishra, and B. Ottersten, "A mmWave automotive joint radar-communications system," *IEEE Trans. Aerospace and Electronic Sys.*, vol. 55, no. 3, pp. 1241-1260, June 2019.
- [18] X. Lv, J. Wang, Z. Jiang, and W. Wu, "A joint radar-communication system based on OCDM-OFDM scheme," in *Proc. IEEE Int. Conf. on Microwave and Millimeter Wave Tech.*, May 2018, pp. 1-3.
- [19] L. G. de Oliveira, M. B. Alabd, B. Nuss, and Th. Zwick, "An OCDM radar-communication system," in *14th European Conf. on Antennas and Propagation*, Mar. 2020, pp. 1-5.
- [20] S. Bhattacharjee, K. V. Mishra, R. Annavajjala, and C. R. Murthy, "Evaluation of orthogonal chirp division multiplexing for automotive integrated sensing and communications," *IEEE Int. Conf. Acoustics, Speech and Signal Proc. (ICASSP)*, May 2022, pp. 8742-8746.
- [21] S. Mercier, S. Bidon, D. Roque, and C. Enderli, "Comparison of correlation-based OFDM radar receivers," *IEEE Trans. Aerospace and Electronic Sys.*, vol. 56, no. 6, pp. 4796-4813, Dec. 2020.
- [22] Y. Jing, J. Liang, B. Tang and J. Li, "Designing unimodular sequence with low peak of sidelobe level of local ambiguity function," *IEEE Trans. Aerospace and Electronic Sys.*, vol. 55, no. 3, pp. 1393-1406, June 2019.
- [23] T. Tsao, M. Slamani, P. Varshney, D. Weiner, H. Schwarzlander, and S. Borek, "Ambiguity function for a bistatic radar," *IEEE Trans. Aerospace and Electronic Sys.*, vol. 33, no. 3, pp. 1041-1051, July 1997.
- [24] A. Freedman and N. Levanon, "Properties of the periodic ambiguity function," *IEEE Trans. on Aerospace and Electronic Sys.*, vol. 30, no. 3, pp. 938-941, July 1994.
- [25] N. Levanon, "The periodic ambiguity function - Its validity and value," *IEEE Radar Conf.*, May 2010, pp. 1-5.
- [26] J. Wang, B. Zhang, and P. Lei, "Ambiguity function analysis for OFDM radar signals," *CIE International Conference on Radar*, Oct. 2016, pp. 1-5.
- [27] J. Mietzner, "DFT-spread OFDM MIMO-radar - an alternative for reduced crest factors," *20th Int. Radar Symp.*, June 2019, pp. 1-10.
- [28] J.-Y. Nieh and R. A. Romero, "Comparison of ambiguity function of eigenwaveform to wideband and pulsed radar waveforms: a comprehensive tutorial," *The Journal of Engineering*, vol. 2018, no. 4, pp. 203-221, 2018.
- [29] J. J. Benedetto, I. Konstantinidis, and M. Rangaswamy, "Phase-coded waveforms and their design," *IEEE Signal Proc. Mag.*, vol. 26, no. 1, pp. 22-31, Jan. 2009.
- [30] J. J. Benedetto and J. J. Donatelli, "Ambiguity function and frame-theoretic properties of periodic zero-autocorrelation waveforms," *IEEE J. Sel. Topics Signal Proc.*, vol. 1, no. 1, pp. 6-20, June 2007.
- [31] A. Kebo, J. Konstantinidis, J. J. Benedetto, M. R. Dellomo, and J. M. Sierackit, "Ambiguity and sidelobe behavior of CAZAC coded waveforms," *IEEE Radar Conf.*, April 2007, pp. 99-103.
- [32] B. M. Popović, "Generalized chirp-like polyphase sequences with optimum correlation properties," *IEEE Trans. Inf. Theory*, vol. 38, no. 4, pp. 1406-1409, July 1992.
- [33] *Physical channels and modulation; (Release 17)*, document 3GPP TS38.211 V17.0.0, Dec. 2021. [Online]. Available: <https://www.3gpp.org>
- [34] R.-A. Pitaval, B. M. Popović, P. Wang, and F. Berggren, "Overcoming 5G PRACH capacity shortfall: supersets of Zadoff-Chu sequences with low-correlation zone," *IEEE Trans. Commun.*, vol. 68, no. 9, pp. 5673-5688, Sept. 2020.
- [35] P. Wang and F. Berggren, "Secondary synchronization signal in 5G New Radio," *IEEE Int. Conf. Commun.*, May 2018, pp. 1-6.
- [36] G. E. A. Franken, H. Nikookar, and P. van Genderen, "Doppler tolerance of OFDM-coded radar signals," *3rd European Radar Conf.*, Sept. 2006, pp. 108-111.
- [37] R. Saadia and N. M. Khan, "Single carrier-frequency division multiple access radar: waveform design and analysis," *IEEE Access*, vol. 8, pp. 35742 - 35751, Feb. 2020.
- [38] S. Sen, "PAPR-constrained pareto-optimal waveform design for OFDM-STAP radar," *IEEE Trans. Geoscience Remote Sensing*, vol. 52, no. 6, pp. 3658-3669, June 2014.

- [39] X. Lv, J. Wang, Z. Jiang, and W. Jiao, "A novel PAPR reduction method for OCDM-based radar-communication signal," *IEEE MTT-S International Microwave Workshop Series on 5G Hardware and System Technologies*, Aug. 2018, pp. 1-3.
- [40] A. Aubry, A. De Maio, B. Jiang, and S. Zhang, "Ambiguity function shaping for cognitive radar via complex quartic optimization," *IEEE Trans. Signal Proc.*, vol. 61, no. 22, pp. 5603-5619, Nov., 2013.
- [41] G. Cui, Y. Fu, X. Yu, and J. Li, "Local ambiguity function shaping via unimodular sequence design," *IEEE Signal Proc. Lett.*, vol. 24, no. 7, pp. 977-981, Jul., 2017.
- [42] L. Pralon, G. Beltrao, B. Pompeo, M. Pralon, and J. M. Fortes, "Near-thumbtack ambiguity function of random frequency modulated signals," *IEEE Radar Conf.*, May 2017, pp. 352-355.
- [43] B. M. Popović, "Optimum sets of interference-free sequences with zero autocorrelation zones," *IEEE Trans. Inf. Theory*, vol. 64, no. 4, pp. 2876-2882, Apr. 2018.
- [44] B. M. Popović, "Efficient DFT of Zadoff-Chu sequences," *IEE Electronics Letters*, vol. 46, no. 7, pp. 502-503, 2010.
- [45] R. H. Clarke, "A statistical theory of mobile-radio reception," *The Bell Syst. Tech. J.*, pp. 957-1000, Jul.-Aug., 1968.
- [46] Y. Zeng, Y. Ma, and S. Sun, "Joint radar-communication with cyclic prefixed single carrier waveforms," *IEEE Trans. Veh. Technol.*, vol. 69, no. 4, pp. 4069-4079, Apr. 2020.